Computational Strategy in Catalyst Design

Thesis by

Robert J. Nielsen

In Partial Fulfillment of the Requirements

for the Degree of

Doctor of Philosophy

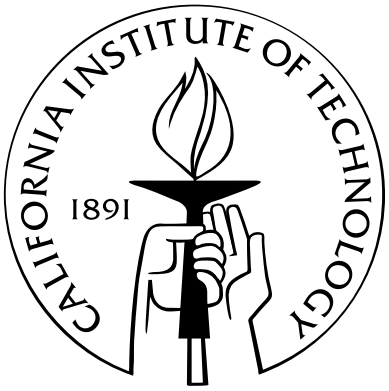

California Institute of Technology

Pasadena, California

2005

(Defended June 2, 2005)

Acknowledgements

I thank Bill Goddard for teaching me his way of thinking about metals and his optimistic support.

I thank Jason Keith, with whom I collaborated while resolving the mechanism of alcohol oxidation by ((–)-sparteine)PdX_2 (section 2.3), and who is now investigating the interaction of O_2 and reduced palladium species.

I thank Professor Brian Stoltz and his students Raissa Trend and Eric Ferreira for sharing their insights into palladium-catalyzed oxidations, and especially Jeff Bagdanoff for investing effort in synthesizing new ligands (section 3.3) developed in the course of the theoretical investigations.

The computational facilities at the Materials and Process Simulation Center were funded by grants from ARO-DURIP, ONR-DURIP, IBM-SUR, and the Beckman Institute. I have graciously been supported by grants from the NSF and Chevron-Texaco Energy Research and Technology Company.

Abstract

The strategy and efficacy of applying computational tools to the development of new catalytic cycles is discussed using the enantioselective palladium-catalyzed aerobic oxidation of secondary alcohols as a model case. The key interactions responsible for the unique reactivity of ((–)-sparteine)PdX_2 complexes (X = chloride, acetate) in kinetic resolutions of secondary alcohols are elucidated using density functional theory with the Poisson-Boltzmann polarizable continuum solvent model. Enantioselectivities in these reactions are found to follow directly from calculated energies of diastereomeric beta-hydride elimination transition states incorporating (R) and (S) substrates. This relationship reveals an important role of the anion, namely to communicate the steric interaction of the ligand on one side of the Pd^{II} square plane and the substrate on the other side. When no anion is included, no enantioselectivity is predicted. Locating these transition states in different solvents shows that higher dielectrics stabilize the charge separation between the anion and metal and draw the anion farther into solution. Thus the solvent influences the barrier height (rate) and selectivity of the oxidation.

Based on this understanding, computational assays for selectivity, reaction rate and stability are developed and used to screen possible mimics of the natural product (–)-sparteine which could be synthesized in both antipodes. Derivatives of the bispidine and bispidinone structures are predicted to have high selectivity but poor stability on palladium. Experimental results verify that catalytically active (bispidine)PdX_2 complexes do not form.

Mechanisms by which palladium diacetate complexes of N-heterocyclic carbenes may oxidize alcohols (a reaction known to occur with no enantioselectivity) are examined computationally. The strong trans effect of the carbene distinguishes the behavior of these complexes from other palla-

dium catalysts. No traditional beta-hydride elimination is predicted to be capable of generating the high deuterium kinetic isotope effect measured using this catalyst. Instead, the low-energy pathway consistent with previous experimental observations (KIE, activation parameters, kinetics) is a "reductive" beta-hydride elimination, in which the beta-hydrogen of the alcohol is transferred directly to a bound acetate ligand. Assuming that relative energies of transition states of this type will determine enantioselectivity, new, chiral carbene ligands are hypothesized and screened. Careful placement of stereocenters and steric bulk has led to ligands with high predicted enantioselectivity and stability.

Recurring factors in the induction of selectivity by asymmetric ligands are observed. Strengths and weaknesses of quantum chemistry as applied to catalytic cycles are discussed, along with the synergy of theory and experiment. Common pitfalls and areas in need of improvement are highlighted.

Contents

List of Figures

List of Tables

Chapter 1

Introduction and Methods

1.1 Background

Chemistry continues to resist our attempts to reduce it from an empirical science, where progress comes through chance and wisely directed effort, to an engineering excercise, where new structures for performing desired functions are regularly derived from a set of proven principles. Certainly goals are reached, and the theoretical framework describing chemical structure and reactivity and the experimental techniques to measure them that have developed over the last century allow researchers to direct their investigations along the most promising avenues. But the path to success is often circuitous with unexpected discoveries or setbacks along the way. Other plausible goals, like the efficient conversion of photons to electric or chemical potential or the selective functionalization of alkanes, are still unmet. Sophisticated apparatuses have developed to isolate reactants and control their rates of reaction, crystallography has allowed us to "see" species in a 3-dimensional format easily accessible to our minds, the mathematics of quantum mechanics describes the behavior of simple models, numerous spectroscopies provide information about fleeting chemical intermediates in all phases of matter, and the electronic library supplies an organized history of chemical observations. Despite this, meeting the next technological demand in a chemical, materials science, or biochemical industry is still not a predictable matter of handing the task to a research department or contracting the work to the lowest bidder.

In the category of catalysis, the discrete nature of chemistry means there are no "equations of

catalysis" to be solved to identify the composition of a solid surface or structure of a ligand system (or the method of preparation) required for a new reaction. Here I relate my attempt to fill that gap by using computational chemistry to bridge known catalytic cycles to new cycles we would find useful. The intended role of simulations is to replace iterations through synthesis→evaluation→variation with a more direct link from desired function to required structure.

Though the end goal is to use computers to design catalysts which behave in the real world as they were predicted to behave virtually, computation is intended to complement, not replace, experimental studies. The end of any successful campaign is the demonstration of a working catalyst whose synthesis is not prohibitively complicated. At the beginning of a theoretical study, it behooves us to let experimental observations of known reactions related to the new goal supply us with promising motifs for further analysis. Until modeling can accurately predict the selectivities between all the diverging reaction paths available to substrate, catalyst, and supposed spectators, observed products may tell us which step of a cycle needs more attention. And agreement between measurements and theoretical predictions serves to validate models so that the physical insights they provide can be trusted.

What computational modeling can provide is a means of resolving the atomic-scale workings of observed reactions and predicting the behavior of hypothesized systems. In this way we can explain why the electronic or geometric structure of one catalyst is effective while alternatives are not. Computation provides a cheaper and often faster route to structural and thermodynamic information about proposed intermediates than many spectroscopic techniques (though it is up to the researcher to determine the relevance of the proposed models.) Since the contents and thermodynamic state of a chemical model can be controlled (either explicitly or statistically by Monte Carlo), all the states of a system may be equally amenable to simulation. This allows modelling to compliment investigations of real surfaces which are often restricted to idealized conditions. Varying the chemical composition of a model allows derivatives of reactivity with respect to structure to be measured without investing effort in synthesis. Most importantly, computational chemistry enables the study of molecules which may have interesting properties but for which no close analogue exists experimentally.

A first-principles understanding of physics, especially when aided by modern computing, has made other technological fields predictable to a practical degree. The complex behavior of solids under stress and new materials notwithstanding, much of our infrastructure has been successfully designed to perform to predifined specifications. The command of Newton's laws and solid mechanics allows the construction of daring new buildings with unique functions, with degrees of freedom left to spare on aesthetics. The construction of new bridges cannot proceed iteratively, yet they would not be permitted without a confidence in their performance that goes beyond knowing related structures have performed satisfactorily in the past. In chemistry today, we cannot have the same confidence in a new molecule's performance until it has been verified empirically.

More recently the aerospace industry has benefitted from digitalization of its design and assembly efforts. Creators of the Boeing 777 established a new benchmark in efficiency by using a 3-dimensional computer-aided drawing environment to virtually pre-assemble the aircraft, saving costly redesign and reconstruction [1]. More impressive than simulating the spatial extent of components is the progress in computational fluid dynamics. The Navier-Stokes equations with accompanying turbulence models can be solved to rapidly assess the lift and drag characteristics of an airfoil silhouette or an entire aircraft. While applying this ability iteratively allows today's engineer to choose values for parameters which best meet his needs, methods for the *direct* optimization of 3-dimensional structures are under development.

Catalysis has not experienced the same kind of digital revolution. A primary reason for this is that we have not yet found a combination of ab initio physics and mathematical approximations which affords useful accuracy (kcal/mol) when treating realistically-sized chemical models (100 atoms) in an acceptable time (hours). It is one thing to pay graduate students to pioneer the current possibilities, but making a profit will require better than two out of these three. Also, as the field is still developing, there are no established algorithms for using the tools that do exist to generate the understanding we seek. Such algorithms are one goal of this work.

Any approach to catalysis (rational or combinatorial, experimental or theoretical) must overcome the challenges of designing not just a structure but a *cycle* of interactions balancing multiple and

contradictory properties. An active site, while avoiding poisoning by spectators, must bind reactants and products just strongly enough that both adsorption and desorption events occur on a similar time scale. Recall "volcano" plots revealing a maximum in reaction rate as the constituents of a catalyst traverse the periodic table. In cycles involving redox chemistry, the catalyst at one point in the reaction must be a strong enough oxidant to take electrons from a substrate, yet mild enough to then pass them off to a terminal oxidant to complete the cycle. In general, the overall thermodynamics of the net reaction place bounds on the elementary steps: each step must have a low enough barrier to occur frequently, but not be so exothermic that a thermodynamic sink appears in the middle of the cycle. To avoid deleterious side reactions, cocatalysts, reactants and products must only enter the reaction when expected. To satisfy all these constraints (along with stability and synthesizability), geometric, electronic and solubility properties must all be manipulated within a single molecule or surface.

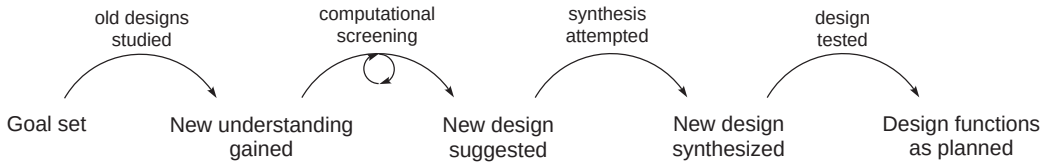

Figure 1.1: Progress in modeling studies of catalysis.

Computational investigations in catalysis, including this work, roughly proceed through the scheme outlined in Figure 1.1. While direct or automated optimization is conceivable in the cases of airfoil design or process engineering, an analytical approach is not even on the distant horizon of computational catalysis. Independent variables in catalytic cycles (the elements, chiefly, but also the sequence of steps and the choice of oxidant, for example) are not continuous. Also, the properties of a cycle we wish to optimize (rates or activation energies, selectivity, atom efficiency) do not depend in a simple way on the given catalyst formulation. While computers are employed to quatitatively describe reaction intermediates, they cannot by themselves tell what steps determine the reaction rate or are likely to lead to undesired reactions. So, progress here has come by understanding known reactions and iteratively applying that understanding to new, related catalysts.

1.1.1 Roadmap

The body of this thesis describes the application of computational chemistry to the palladium-catalyzed kinetic resolution of racemic mixtures of secondary alcohols. The natural product (–)-sparteine was identified by the Stoltz and Sigman groups as an effective ligand on palladium for promoting the aerobic oxidation of (*R*) alcohols to the corresponding ketones at rates 20 to 30 times faster than their (*S*) antipodes. Chapter 2 describes the elucidation of the previously unknown interactions responsible for enantioselectivity. A new, tunable ligand which could be easily synthesized in *both* (+) and (–) enantiomers would increase the substrate scope and permissible reaction conditions of the existing (–)-sparteine protocols. Chapters 3 and 4 therefore describe two approaches to designing a replacement for (–)-sparteine.

Chapter 5 contains a general discussion of insights into the process of extracting useful chemical information from molecular models and habits to follow and avoid. Chapters 2 through 4 are implied as examples here, but illustrations are also drawn from other pursuits. The remainder of this chapter introduces the methods commonly employed in theoretical investigations into catalytic reactions.

1.2 Methods

The computational machinery employed here does not extend beyond tools a researcher could find for sale, in freely distributed software, or perhaps from their friendly neighborhood theorist. The scope of problems which are approachable with the most established techniques is of course smaller than what is being treated by specialists developing methods for specific new phenomena. Even these core computational methods will bear more fruit in experienced hands. But the fraction of questions regularly posed by chemists which we can expect to consistently benefit from the computational component of our arsenal grows as new tools (e.g., for the generation of spectroscopic responses, for incorporating dynamics, for treating realistically sized models, etc.) are proved.

To make progress, a practical approach is taken to the addage that "everything" is available from the quantum mechanical wavefunction of a system. In this work, and others needing to model more

than 10 or 20 atoms, we immediately substitute the electron density for the wavefunction, from which the total energy and highest occupied molecular orbital energy are theoretically available, and much more if we are willing to concede some rigor for the necessary improvement in speed. Since in studying catalysis an accurate description of the making and breaking of covalent bonds is necessary, we begin with *ab initio*[1] models, for which the only input is nuclear coordinates and charges, the total number of electrons, and (in the case of DFT) an ad hoc Hamiltonian to be used in the time-independent Schrödinger equation.

Conceptually more elaborate methods are being developed to describe the inherently quantum-mechanical process of bond breaking in the presence of scores of neighboring atoms whose influence needs to be represented. Reactive forcefields are a self-consistent solution to this problem in which all the atoms in a model are governed by an unchanging list of rules which prescribe the total energy of the system as a function of the atoms' coordinates [2, 3, 4, 5, 6]. Since the mathematical description of each element's bonding characteristics is crafted to reproduce *ab initio* bond dissociation energy profiles, these forcefields succeed in describing reactivity where their non-reactive ancestors failed. While functional forms have been indentified to represent a growing list of interactions (not just spring-like covalent bonds, but delocalization, ferroelectrics [7, 8], etc.), the multivalency of metals has not yet been captured. Also, since the training of the forcefield requires the generation of considerable amounts of *ab initio* data, one might prefer to use that computational effort to directly address the application at hand. An advantage of the forcefield is that it allows a *dynamic* description of a large number of atoms, which may evolve through unexpected mechanisms. Thus one useful strategy is the identification of reaction mechanisms using classical dynamics on an accurate if imperfect potential energy surface, followed by their quantification and understanding through quantum mechanical methods.

Hybrid methods (so-called QM/MM) are also being developed in which a small number of atoms most crucial to an active site are modeled quantum mechanically while surrounding groups which may affect the site sterically or electrostatically are modeled with a forcefield [9, 10, 11]. The

[1] If the reader wishes to withhold this categorization from certain density functionals, the author understands.

surroundings communicate with the quantum region through non-covalent interactions (like those found in a traditional forcefield simulation) and a boundary condition which forces the bonds along the periphery of the quantum region to be colinear with the corresponding bonds in the classical model. Some may find this coupling procedure questionable, and a more seamless approach to including the effects of surrounding atoms is to represent large moieties around the active site by effective potentials which are passed into the Hamiltonian of a quantum mechanical calculation. For instance in biological applications, distant peptides in proteins have been reduced to such a potential, which can be added to the traditional nuclear and electronic potential energy terms [12, 13].

DFT models are used to answer the questions posed in the following chapters. From these static and microscopic pictures, a layering of other disciplines allows chemically relevant information to be constructed. The art of manipulating ensembles of virtual atoms to model real molecules is discussed in Chapter 5, while here some useful quantities afforded by such methods are introduced.

1.2.1 Wavefunctions and Hamiltonians

Ab initio quantum chemical methods seek a many-electron wavefunction which minimizes the energy prescribed by the exact[2] Hamiltonion H

$$H = \sum_{A \neq B} \frac{Z_A Z_B}{R_{AB}} - \sum_{A,i} \frac{Z_A}{r_{Ai}} - \sum_i \frac{1}{2}\nabla^2 + \sum_{i \neq j} \frac{1}{r_{ij}}$$

(where the sums run over nuclei A and electrons i). Increasingly accurate solutions are found by employing more sophisticated and flexible representations of the target wavefunction. The simplest form for an antisymmetric wavefunction (the sign of the wavefunction must change when all the coordinates of two electrons are exchanged) is a Slater determinant of spin orbitals. The single

[2]Here "exact" refers to the time-independent, non-relativistic Hamiltonian under the Born-Oppenheimer approximation, but in which the $\frac{1}{r_{ij}}$ term expressing the repulsion of electrons is left intact.

determinant with the lowest energy is the Hartree-Fock solution to the many-body problem:

$$\Psi_{\mathrm{HF}}(\mathbf{x}_1, \mathbf{x}_2, \ldots, \mathbf{x}_N) = \frac{1}{\sqrt{N!}} \begin{vmatrix} \phi_1(\mathbf{x}_1) & \phi_2(\mathbf{x}_1) & \ldots & \phi_N(\mathbf{x}_1) \\ \phi_1(\mathbf{x}_2) & \phi_2(\mathbf{x}_2) & & \phi_N(\mathbf{x}_2) \\ \vdots & & \ddots & \vdots \\ \phi_1(\mathbf{x}_N) & \phi_2(\mathbf{x}_N) & \cdots & \phi_N(\mathbf{x}_N) \end{vmatrix} = \forall[\phi_1(\mathbf{x}_1)\phi_2(\mathbf{x}_2)\ldots\phi_N(\mathbf{x}_N)]$$

Even if the spin orbitals in such a determinant are constructed from a complete set of basis functions, the energy (and associated geometry) obtained from this procedure is unreliable. The correlation of electrons' positions is not represented in this scheme, save that antisymmetrization guarantees that like-spin electrons will not occupy the same point in space simultaneously.

Electron correlation can be incorporated into the wavefunction by mixing the Hartree-Fock determinant with additional determinants (configurations) in which one or more electrons have been "excited" to molecular orbitals unoccupied in the Hartree-Fock ground state:

$$\Psi_{\mathrm{CI}} = c_0\Psi_{\mathrm{HF}} + \sum_{i,x} c_i^x \Psi_i^x + \sum_{i\neq j, x\neq y} c_{ij}^{xy}\Psi_{ij}^{xy} + \ldots$$

where $\Psi_{12}^{xy} = \forall[\phi_x(\mathbf{x}_1)\phi_y(\mathbf{x}_2)\phi_3(\mathbf{x}_3)\ldots]$ and sums run over spin orbitals occupied in the Hartree-Fock ground state (ϕ_i) and excited states ϕ_x. Interference between the different configurations decreases the probability of finding two electrons in the same region of space. Thus the Hartree-Fock determinant describes a pair of electrons occupying (for example) a bonding orbital as oblivious of each other, while including a perturbative amount of antibonding character allows the configuration interaction wavefunction to describe the same pair of electrons in more detail: the electrons share the same orbital, but when one electron is near the left nucleus, the other is more likely to be near the right nucleus. Including an infinite number of excited configurations allows a perfectly correlated wavefunction to be written.[3]

An accounting of at least the majority of the correlation energy (the difference between the lowest Hartree-Fock and configuration interaction energies) is necessary in thermochemical investigations.

[3]For more discussion of ab initio methods, see [14].

The correlation energy in modest H_2 is over 20 kcal/mol, and one can expect to incur O(10 kcal/mol) errors per bond by neglecting correlation during reactions. Unfortunately the computational expense of including a sufficient number of excited configurations leaves most molecules outside the reach of accurate treatment.

An alternative to ab initio methods are *density functional* methods, which seek accurate total energies by applying increasingly sophisticated operators to a simple representation of the electronic density. In theory a functional exists which extracts the exact total energy from a given 3-dimensional electronic density, but this functional remains unknown. Instead, a $3N$-dimensional density (again a single Slater determinant of N electrons) is often used so that known operators like those for kinetic and exchange energy can be employed and the more elusive contributions to the total energy limited to contrived functionals. In practice, such functionals (of the density and its spatial gradient) are constructed to satisfy analytical constraints or reproduce observed phenomena.[4]

In this work the collection of gradient-corrected density functionals known as B3LYP is used to evaluate the contributions of exchange and correlation to the total energy. Motivated by the deficiencies of semiempirical exchange functionals in describing bond strengths, Becke [17] showed that an optimally weighted combination of exact exchange with LSDA (linear spin density approximation) and gradient-corrected exchange functionals was able to reproduce the atomization energies of small molecules to within a few kcal/mol. The resulting "B3" exchange functional has been combined with Lee, Yang, and Parr's correlation functional [18], a recasting of Colle and Salvetti's [19] formula for correlation energy in terms of the electronic density. The earlier authors wrote a corellated wavefunction as the product of a Hartree-Fock determinant and factors which decrease the amplitude as two electrons approach one another:

$$\Psi_{\mathrm{C-S}}(\mathbf{x}_1, \mathbf{x}_2, \ldots) = \Psi_{\mathrm{HF}}(\mathbf{x}_1, \mathbf{x}_2, \ldots) \prod_{i \neq j} (1 - e^{-\beta^2 (\mathbf{r_i} - \mathbf{r_j})^2} \Phi(\mathbf{r_i}, \mathbf{r_j}))$$

After mathematical simplifications and assigning values to a few parameters using an accurate treatment of the He atom only, a formula for the correlation energy of this general wavefunction in

[4] For more discussion of DFT methods, see [15] and [16].

terms of the density and Hartree-Fock second-order density matrix was obtained.

As expected from its calibration, the B3LYP functional's dominant strength is its description of thermochemistry across the periodic table. Geometries are also of high quality compared to those of other density functionals and most wavefunction-based techniques [16]. Weakly bound van der Waals complexes are not well described [20].[5] Since dispersion forces do not dominate in catalysis, this is an acceptable shortcoming.

1.2.2 Building Up Chemical Information

The quantum mechanical energy ("E" throughout) is the natural product of solving the eigenvalue problem associated with the chosen Hamiltonian and includes the nuclear repulsion, electron-nuclear attraction, electron kinetic energy, Hartree electron-electron repulsion, and electronic exchange and correlation energy (to whatever extent exchange and correlation are represented). This energy and the temperature-dependent thermodynamic functions are the first guide to determining the probability of finding a system in one state relative to another during the course of a reaction (but not the probabililty that either state represents reality.) Energies allow the prediction of observables (activation barriers, ratios of rates and concentrations) which are important for validating proposed models when experimental data exists and predicting the behavior of hypothesized structures. The electron distribution is also available at this point, represented commonly as an electrostatic potential, atomic Mulliken charges [21], or explicit orbital amplitudes. This information underpins a "frontier orbital" sense of reactivity, describes the location of lone-pair or unpaired electrons, and allows us to understand whether a reaction is, for example, allowed or forbidden by symmetry, or oxidative or reductive in character.

First derivatives of the energy with respect to nuclear coordinates allow the determination of minimum-energy structures. These illustrate, often for fleeting intermediates, which chemical groups are competing for the same space and what structural modifications should enhance or relieve such strain. Also, differences in predicted structural parameters can serve as indicators of electronic

[5] For example, a purely repulsive potential between noble gas dimers is predicted.

structure, as do structures from x-ray data. Second derivatives of the energy aid in the location of transition states (saddle-points on the potential energy surface) and can be parsed to give the vibrational spectrum of a structure. Transition state structures, combined with their energies and electron distributions, can provide rich explanations for how changes in reactants affect rates or selectivities among a series of analogous reactions.

When modeling reactions performed in solution, a representation of the solvent must be included if one desires more than qualitative insight. In cases where the solvent does not participate as a reactant, and since in a static model its role as a thermal bath is irrelevant, the leading role of the solvent is that of a dielectric medium which allows the electronic and geometric structure of a solute to relax from its *in vacuo* form. Therefore a useful model of the solvent is a polarizable continuum, with the experimentally determined dielectric constant, surrounding the explicit solute at a distance determined by the van der Waals radii of the solute and solvent. After the gas-phase wavefunction for the solute has been obtained, the Poisson equation can be solved to determine the charge distribution which would form at the solute-solvent interface in response to the solute's electrostatic potential. These charges can be added to the solute Hamiltonian and a new, polarized wavefunction generated. These two steps are repeated until wavefunction and charges are self-consistent (Figure 1.2). This process of *electronic* relaxation often (in low-dielectric media) accounts for the solvation energy of a model. However, derivatives of the new Hamiltonian include the forces on atoms due to the solvent, so *solvent-optimized structures* can be determined. Since many intermediates a chemist might be interested in are not stable in the gas phase (i.e., ionic or zwitter-ionic compounds), the solvent model's ability to stablize charge separation is crucial for finding realistic geometries of species in solution. Also, the effects of different solvents on the description of a reaction can be followed by applying the appropriate dielectric constants and effective solvent radii.

Formulas of statistical mechanics are used to translate quantum mechanically derived quantities (energy and vibrational frequencies) into thermodynamic functions and measurable chemical properties. Accurate vibrational, rotational and translational partition functions for ideal gases follow from the quantum mechanical harmonic oscillator, rigid rotator, and free particle approximations.

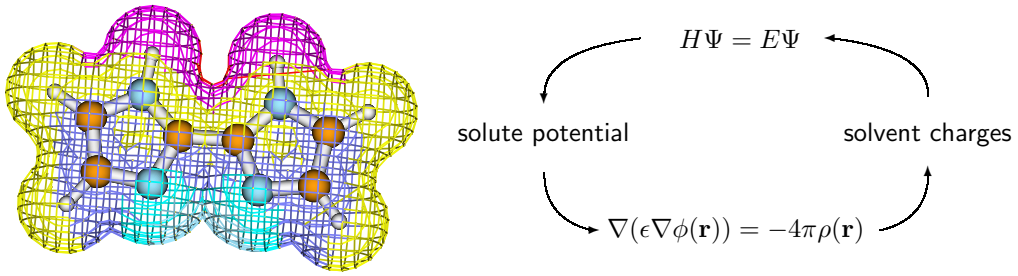

Figure 1.2: The electrostatic potential around 2,2'-biimidazole and the iterative routine for including solvation in a quantum mechanical simulation using the polarizable continuum method.

Liquid phase thermodynamics, particularly entropy, are less accessible from a treatment of an isolated molecule which has no representation of the "cage" potential provided by the surrounding fluid. Fortunately, this potential is much softer than that governing intramolecular modes[6], so the contributions of the external degrees of freedom (hindered translation and rotation) to enthalpy are expected to saturate to their classical limit of $\frac{1}{2}$kT. The low-frequency limit of vibrational entropy, however, is not so well behaved. Estimates of liquid phase entropies can be made by analogy to tabulated experimental values or calculated from molecular dynamics simulations.

In cases where relative free energies of intermediates and transition states can be calculated, transition state theory is used to estimate reaction rates. Rate constants of elementary steps are based on the free energy change between a transition state and the preceeding stable intermediate which contains all of the same atoms. Calculation of observed reaction rates and activation parameters requires the correct rate expression for the catalytic cycle and knowledge of which intermediates dominate the population. This information must be assembled from the relative free energies of the various intermediates and any reaction orders observed for reactants. Ratios of calculated rates are useful for comparison to selectivity or kinetic isotope effect data, and are likely to benefit from a cancellation of error in frequency factors or activation entropies.

Table 1.1 provides sample thermodynamic calculations of the type found within using species

[6]The presence of a hydrogen bonding network may invalidate this approximation.

Table 1.1: Sample thermodynamics calculations

		Calc.[1]	Exp.[2]	Calc.	Exp.
		E.A. (eV)		I.P. (eV)	
1	Pd (atom)	-0.08(-0.26[3])	-0.56	8.67(8.67[3])	8.40
		ΔH° (kcal/mol)		ΔE_{sol}	
2	$PdCl_4^{2-}(aq) + Cl_2(g) \rightarrow PdCl_6^{2-}(aq)$	-8.6(-11.3[3])	-11.4	-9.5	
3	$\text{toluene}(l) + H_2O(l) \rightarrow \text{benzene}(l) + CH_3OH(l)$	15.7	20.1	14.9	
4	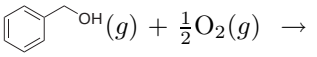	-42.0	-44.0	-40.3	
		ΔH° (kcal/mol)		ΔS° (cal/mol·K)	
5	$H_2O(g) + \frac{1}{2}O_2(g) \rightarrow H_2O_2(g)$	26.0	25.3	-15.4	-14.0

[1]B3LYP using double-ζ basis sets of Pople [22, 23, 24] with diffuse functions on O and Cl atoms and the Los Alamos pseudopotential for palladium [25] with valence functions contracted to double-ζ [2]Thermodynamic properties are taken from [26] and [27] [3]Calculated with the valence functions of palladium contracted to triple-ζ

whose thermodynamic properties have been tabulated. The enthalpy of a species is calculated as:

$$\mathrm{H} = \mathrm{E}_{elec} + \mathrm{G}_{solv} + \sum_{\nu} \frac{1}{2} h\nu + \frac{n}{2}\mathrm{kT} + \sum_{\nu} \frac{h\nu}{e^{h\nu/\mathrm{kT}} - 1} \tag{1.1}$$

including the total energy from the electronic structure calculation, the solvation energy[7] based on the solution of Poisson's Equation around liquid-phase species, the zero-point energy, contributions of $\frac{1}{2}$kT for each rotational and translational degree of freedom and one kT for the PV contribution to the enthalpy of gas-phase species, and finally the enthalpy of the vibrational modes. In some instances a solvated energy, $\mathrm{E}_{sol} = \mathrm{E}_{elec} + \mathrm{G}_{solv}$, will be discussed. This quantity contains the components of enthalpy which do not require the time consuming calculation of second derivatives and vibrational frequencies and provides a quick estimate of enthalpy.

Entries 1 and 2 show that finite basis sets commonly used are by no means converged (compare the results from the double- and triple-ζ contractions of palladium's valence functions). Additional precision is gained by employing larger bases, particularly on species whose electron density changes greatly during a reaction. The polarizable continuum solvation model has proven effective for high and low dielectric media, although for the sake of calculating enthalpy changes reaction 2 was

[7]Calculated solvation energies based on an empirical dielectric constant are *free* energies. The difference between solvation enthalpy and free energy can be problematic when treating ionic species in high-dielectric media (see Section 5.2).

purposely chosen to maintain the number of ionic species. High dielectric media are not considered in the body of this thesis, but the shortcomings of treating ionic species in high dielectric media are discussed in section 5.2.

Chapter 2

Enantioselective Oxidation of Secondary Alcohols by ((–)-Sparteine)PdX_2

2.1 Introduction

[1] Recent examples of alcohol oxidations by Pd^{II} complexes and molecular oxygen, in the absence of copper co-catalysts, demonstrate increasing efficiency and selectivity. Generally, the metal (ligated to sp^2 [28, 29, 30] or sp^3 [31, 32] nitrogen, DMSO [33, 34] or a carbene [35], and common anions) and a catalytic amount of base enable the dehydrogenation of an organic substrate by O_2, producing water or hydrogen peroxide[2].

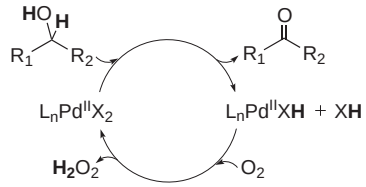

A subset of these reactions is the enantioselective oxidation of secondary alcohols to ketones by a ((–)-sparteine)PdX_2 catalyst (X = Cl, OAc), generating primarily H_2O_2. Sparteine, an asymmetric natural product able to coordinate to Pd by two sp^3-nitrogen lone pairs, has engendered relative rates between (R) and (S) enantiomers of model aryl substrates of up to 47:1 [31, 32]. The aim of

[1] Reproduced with permission from *J. Am. Chem. Soc.* **2004**, *126*, 7967. Copyright 2004 American Chemical Society.

[2] For more on non-enantioselective palladium catalysts for aerobic alcohol oxidation, see section 4.1

this chapter is to trace the observed characteristics of this catalyst, and less effective ones, to their microscopic causes.

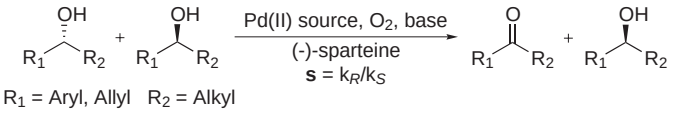

Organic chemists often seek the simplest synthetic route to large, biologically active molecules whose stereochemistry is critical. Beginning a synthesis from a widely available, enantio-pure source is not always possible. If the shortest synthesis starts from a racemic mixture (or if a stereocenter is generated unselectively along the way), then at some point the unwanted enantiomer must be removed. A kinetic resolution, in which an optically active catalyst promotes the destruction of one antipode much faster than the other, allows the separation of enantiomers with identical physical properties. Enantioselective oxidations of alcohol groups by ((–)-sparteine)PdX_2 have already proved useful in the synthesis of Prozac, Singulair, etc. [36, 37].

Screens by the Stoltz [31] and Sigman [32] groups showed that an array of natural and synthetic ligands exhibit a wide range of reaction rate and enantioselectivity in kinetic resolutions. Only (–)-sparteine exhibited useful enantioselectivity factors (hereafter simply selectivity[3], $\mathbf{s} = k_r/k_s$). As the protocol has been refined, systematic variations in the reactivity of (–)-sparteine-PdX_2 complexes as a function of substrate have been mapped [38]. Basic additives such as Cs_2CO_3 have been found to accelerate turnover [39], presumably by aiding the deprotonation of the alcohol. A recent solvent screen [40] has shown chloroform offers rates and selectivites exceeding those previously measured in toluene. We used the specific kinetic data to guide our investigations, which in turn have revealed the atomistic factors that must be present to allow a ligand's potential selectivity to evidence itself. Using 1-phenylethanol as a representative substrate, we examine the mechanism by which (–)-sparteine-$PdCl_2$ functions. Enantioselectivity is then considered, followed by the consequences of changing anions and solvents.

[3]Pd-catalyzed oxidations have been known to overoxidize primary alcohols to carboxylic acids [29], but we will not be interested in the selectivity between ketone and acid products.

2.2 Methods

Reported solution phase energies (E_{sol}, page 13) are the sum of gas phase electronic energies and solvation energies computed with the Poisson-Boltzmann reactive field method. The gas phase energy is evaluated with the B3LYP [17, 18] collection of gradient-corrected density functionals using a 6-31G** [22, 23, 24] basis set for light atoms (with diffuse functions added to Cl atoms and O atoms in acetate groups), the LACVP [25] relativistic effective core potential for Pd (which treats the 4s, 4p, 4d, 5s and 5p electrons explicitly[4]), and the LAV3P [41] relativistic effective core potential for I (5s and 5p explicit) augmented with a d-polarization shell[5] as optimized by Höllwarth et al [42]. The solvation energy is the difference between solvated and unsolvated calculations performed with the described basis set sans diffuse functions. Solvents were represented with the following parameters: toluene, $\epsilon = 2.379$, probe radius (r_p) = 2.762 Å; chloroform, $\epsilon = 4.806$, r_p = 2.514 Å; 1,2-dichloroethane, $\epsilon = 10.65$, r_p = 2.513 Å. Generally the gas phase structures were used in the solvation calculations. In some cases (the relative energies in Table 2.1), the forces on the atoms from the reaction field of the solvent were used to optimize the structure of the solvated complex, allowing us to follow more precisely the effects of the dielectric. In such cases the relative energies are simply energy differences between solvent-optimized structures.

Stable intermediates are completely relaxed, while transition states are characterized by no interatomic forces and the presence of exactly one imaginary vibrational frequency. When a transition state structure included a displaced anion, we often were not able to eliminate an imaginary frequency corresponding to the relative motion of the unbound fragments (in addition to the imaginary frequency of the reaction coordinate). This probably results from numerical approximations in the methods which make it difficult to completely relax the very soft modes associated with such a loosely bound complex. However, such modes lead to very low force constants and cause only a negligible deviation in the transition state energy.

All calculations were performed with Jaguar 4.0 and 5.0 [43]

[4] Basis functions for the valence electrons were contracted to double-ζ. The energies of key species were also evaluated with f-polarization functions on Pd. Since these functions served to change relative energies among intermediates by less than 0.2 kcal/mol, they were not employed.

[5] Omitting d-functions on I yielded relative energies differing by over 2 kcal/mol.

2.3 Mechanism

2.3.1 General

Discussions of mechanisms for alcohol oxidations by palladium usually invoke a β-hydride elimination from a Pd-alkoxide formed by substrate coordination and deprotonation. Rather than study an assumed sequence of intermediates, the mechanism for the reaction of interest was determined by hypothesizing and testing many routes, using the predicted energetics to eliminate unlikely steps. 1-phenylethanol, free sparteine, and (sparteine)$PdCl_2$ in toluene were taken as reactants (the reference state for energies).

Paths involving oxidative addition to form Pd^{IV} species were found to be quite unfavorable. The products of O-H (**2**) and C-H (**3**) addition lie 58 kcal/mol above the reactants or are altogether unstable (Figure 2.1).

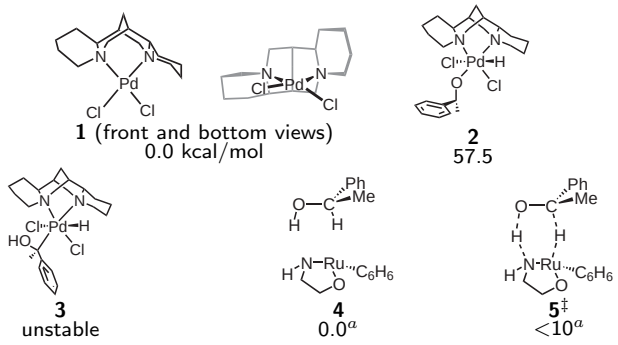

Figure 2.1: ((–)-sparteine)$PdCl_2$ and intermediates unlikely to participate in the oxidation mechanism. Energies (kcal/mol) for **1**-**3** are relative to **1** and include PB solvation by toluene ($\epsilon = 2.379$). [a]From reference [44].

A slightly more feasible route comes by analogy to the ruthenium catalyst of Noyori et al. [45], generated from $RuCl_2(\eta^6$-benzene), β-amino alcohols or *N*-tosyl-1,2-diamines, and strong base. That complex (represented by **4**) performs the same net transformation, *sec*-alcohol to ketone, in one pericyclic step, $\mathbf{5}^{\ddagger}$. Yamakawa's calculations [44] suggest a barrier of less than 10 kcal/mol must be overcome when reacting methanol with the coordinatively unsaturated compound **4**. There are two striking differences, however, between the Ru^{II} and Pd^{II} complexes: the unsaturation of the Ru atom allows it to immediately accept hydride from the alcohol, and the amido nitrogen can accept a proton

without significant geometric rearrangement. No analogous transition state was found involving the Pd^{II} compound, regardless of which base accepted the alcoholic proton: Cl^- dissociating from Pd, a nitrogen of sparteine dissociating from Pd, or exogenous amine. The structures sampled during the search for a concerted mechanism lie more than 30 kcal/mol above the reactants, suggesting that the reaction on Pd consists of some combination of elementary steps.

Many possible paths involving coordination of alcohol, deprotonation, and C-H activation by β-hydride elimination are imaginable if one allows both Cl and sparteine to be displaced from the metal during the reaction. The lowest-energy route through these steps is plotted in Figure 2.2, along with some energetically competitive alternatives[6]. The alcohol enters the coordination sphere by associative substitution for a Cl^- ion (**1**, **6**‡, **7**). The predicted barrier for this displacement ($\Delta E^‡_{sol}$ = 3.8 kcal/mol) is lowered by the $Cl^- \cdots$H–OR hydrogen bond which forms as the substrate approaches. The free Cl^- ion in **7** is not basic enough to deprotonate the bound alcohol alone, but the combination of Cl^- and an exogenous sparteine molecule is. Deprotonation of the coordinated alcohol by free sparteine has not been simulated (due to the large number of atoms and soft degrees of freedom associated with a second, unbound ligand) but the energetic barrier of this step is believed to be much smaller than that of the subsequent β-hydride elimination. (Such is the case for benzyl alcohol [38].) The products of deprotonation in the models are the bound alkoxide **8** and a separate sparteine-H^+Cl^- ion pair, which is predicted to be more stable than separate HCl and sparteine by ΔE_{sol} = 25.2 kcal/mol. The relevance of structure **8** as an intermediate is supported by the recent x-ray characterization of an analogous species (in which the methyl group of the substrate is fluorinated) with the same structure [46].

The alkoxide **8** is found to undergo β-hydride elimination through a 4-coordinate transition state **9**‡, in which the remaining Cl atom is displaced to an axial, outer-sphere position 3.00 Å from Pd (Figure 2.3). The ketone produced (in **10**) is assumed to be easily replaced by the Cl atom, generating the more stable Pd-hydride complex **11**. A 5-coordinate transition state was sought in which the Cl atom remains bound and the β-hydrogen approaches Pd from out of the square plane

[6]Substitution of the alcohol for the other Cl, rotation around the alcohol's O-C bond, and use of (S)-1-phenylethanol lead to energy differences of up to 2 kcal/mol in structures 6-10.

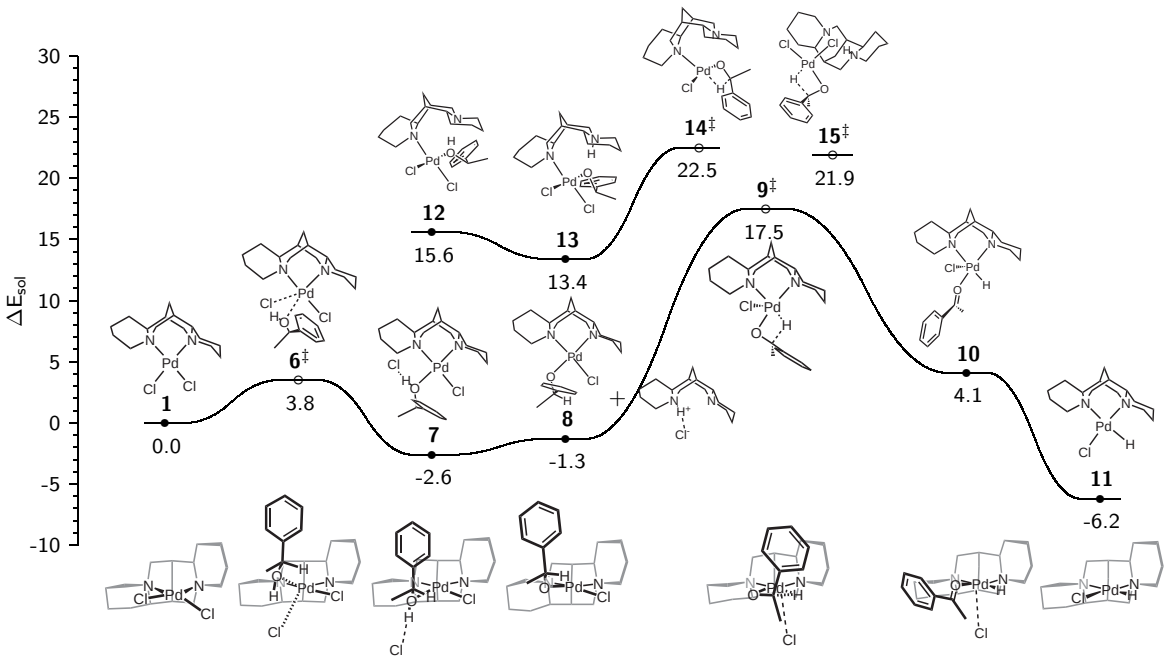

Figure 2.2: Mechanism for the oxidation of (*R*)-1-phenylethanol by ((−)-sparteine)$PdCl_2$. Energies (kcal/mol) are relative to **1** and include PB solvation by toluene ($\epsilon = 2.379$). Images are projections of the 3D structures, with corresponding bottom views aligned below.

to replace the Pd-O bond. That such a structure could not be found is consistent with the fact that palladium's d-orbitals are correctly organized to allow a "2+2" metathesis reaction in the 4-coordinate geometry $\mathbf{9}^{\ddagger}$, but not in a 5-coordinate geometry [47]. Attempts to find a 5-coordinate transition state relaxed to the 4-coordinate structure by displacing the Cl atom from the metal.

It is most intuitive to assume that the sparteine ligand imparts chirality to the metal center by remaining bidentate throughout the reaction and breaking the symmetry of the coordination sphere. Nonetheless we also considered the dissociation of one or both N atoms of sparteine. A general result of the calculations is that the proximity of the nitrogen lone pairs and the bulk and rigidity of the ligand render it possible but unfavorable for sparteine to be bound to palladium by only one nitrogen. This is borne out by the peripheral structures in Figure 2.2. **12**-$\mathbf{14}^{\ddagger}$ belong to a mechanism featuring monodentate sparteine, and a low-energy β-hydride elimination transition state $\mathbf{15}^{\ddagger}$ was found in which both Cl atoms remain bound to Pd while protonated sparteine is present as a counter-ion. Besides being energetically less favorable than $\mathbf{9}^{\ddagger}$, a mechanism including $\mathbf{14}^{\ddagger}$ or $\mathbf{15}^{\ddagger}$ likely suffers kinetically since sparteine must be removed from the metal. We speculate that

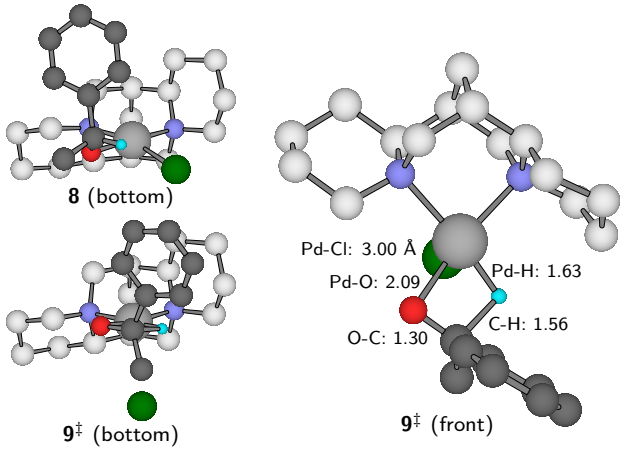

Figure 2.3: Pd-alkoxide **8** and β-hydride elimination transition state $\mathbf{9}^{\ddagger}$. Sparteine carbon atoms in light grey, chlorine in green.

sparteine possesses unusual kinetic stability; in addition to its chelation, its bulk hinders associative substitution mechanisms and its rigidity hinders stepwise breaking of the N-Pd bonds. Finally, these alternate paths are not predicted to yield the enantioselectivities observed experimentally (vida infra).

The reoxidation of L_2PdXH species to L_2PdX_2 by O_2, a reaction general to many catalytic cycles besides the present one, warrants separate attention. This step is apparently not rate-limiting in oxidations featuring nitrogen-bound ligands under an oxygen atmosphere, and presently we find either of two suggestions plausible. O_2 may add across the Pd-H bond in **11** to produce a hydroperoxide complex, as proposed previously [28, 48]. Keith et al. [49] found a specific mechanism for this transformation with a low (12 kcal/mol) activation enthalpy (Figure 2.4 (a)). The oxidizing power of O_2 drives the abstraction of the hydrogen atom from **11** yielding a Pd^{I}-OOH diradical (**23**), which can cross over to the singlet surface through a thermal perturbation of the Pd-O-O-H dihedral angle. The hydroperoxide complex **22** is expected to readily join the **1**⇌**7**⇌**8** equilibrium after protonation by a new alcohol or sparteine-H^+Cl^- and liberation of H_2O_2. Alternatively, Stahl [50] has demonstrated that (bc)$Pd^0(\eta^2$-olefin) (bc = bathocuproine) yields (bc)$Pd^{II}X_2$ and H_2O_2 (via a stable (bc)$Pd^{II}(\eta^2$-peroxo) intermediate) upon attack by molecular oxygen and an acid, HX. An analogous reduced species such as **24** might be attained by deprotonation of **10** and simultaneous production of another equivalent of (–)-sparteine-H^+Cl^-. The starting material **1** could then

be regenerated as demonstrated experimentally and theoretically [51].

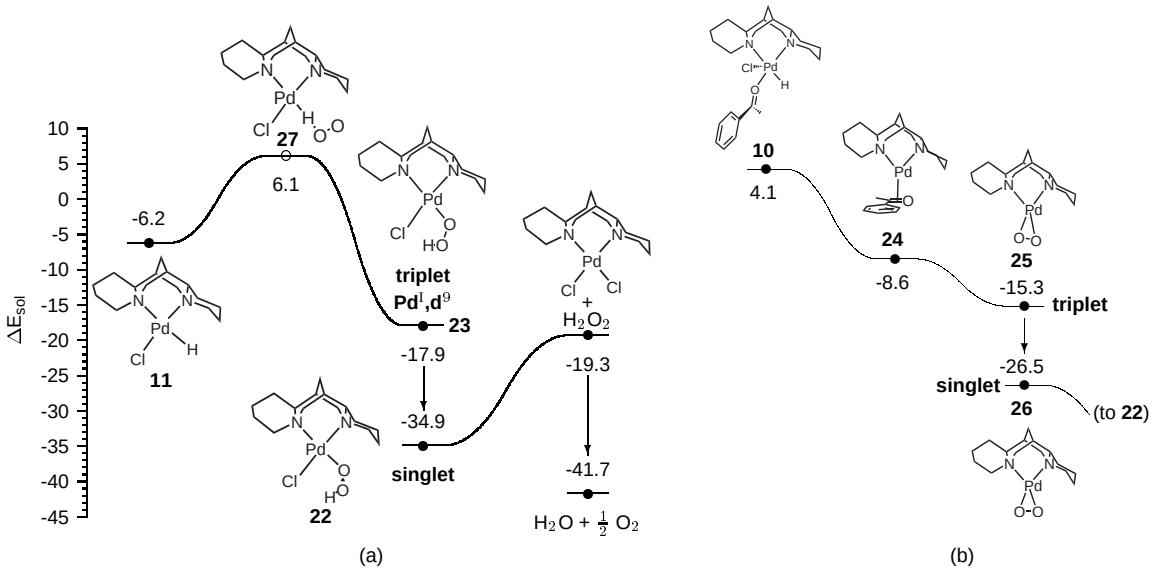

Figure 2.4: Reoxidation of the palladium-hydride intermediate through (a) Pd^{I} and (b) Pd^{0} intermediates. Energies (kcal/mol) are relative to **1** and include PB solvation by toluene ($\epsilon = 2.379$.)

The result of our studies is a mechanism that involves the same sequence of steps proposed by Mueller et al. [52], whose observations of the same model reaction strongly support rate limitation by either deprotonation (at low sparteine loading) or β-hydride elimination (at high sparteine loading). Mueller found no reaction when no excess ligand was present, but as sparteine was added the rate approached an asymptote at high loading. Also, when the β-hydrogen of 1-phenylethanol was replaced with deuterium, Mueller observed a kinetic isotope effect only under sparteine-saturated conditions. In light of these observations, we focus on the deprotonation (DP) and β-hydride elimination (βHE) elementary steps, their dependence on the catalyst's composition, and their control of the observed selectivity.

2.3.2 Chloride vs. Acetate

The thermodynamics in Figure 2.2 suggest that deprotonation of **7** is driven by the concentration of reactants, not by an energetic force. As mentioned, excess sparteine (or other base) is required for reaction to occur using a dichloride Pd source. When $^{-}$OAc replaces Cl^{-} in the catalyst, however,

the calculations predict that the $^{-}$OAc group displaced by the substrate deprotonates the alcohol directly, without the aid of an exogenous base (Figure 2.5). No stable analogue of structure **7** containing $^{-}$OAc was found; instead the proton hops from the alcohol to the acetate ion during the energy minimization. We find that the alkoxide **17** is more stable (ΔE_{sol} = -1.9 kcal/mol) than the sparteine-Pd(OAc)$_2$ starting material **16**. (Again we consider that the acetic acid generated forms a hydrogen-bound complex with free sparteine, predicted to be only 10.2 kcal/mol more stable than separate acetic acid and sparteine.) Consequently we expect the alkoxide to play a larger role in the **16**⇌**17** equilibrium when $^{-}$OAc replaces Cl^{-}, leaving the overall reaction rate to be determined by the β-hydride elimination step at a lower concentration of base. This effect of acetate's greater basicity is confirmed by the observation of modest reactivity when employing (sparteine)-Pd(OAc)$_2$ with no added base [38].

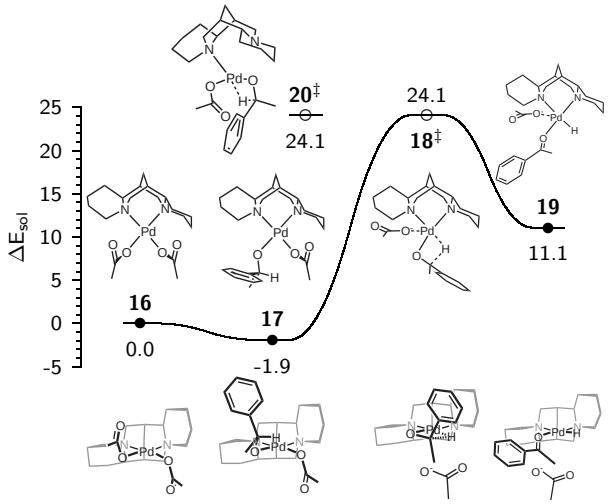

Figure 2.5: Abbreviated mechanism for the oxidation of (*R*)-1-phenylethanol by ((−)-sparteine)Pd(OAc)$_2$. Energies (kcal/mol) include PB solvation by toluene (ϵ = 2.379.) Bottom views are aligned below.

βHE transition state structures and energies were found for 1-phenylethanol incorporating both Cl^{-} and $^{-}$OAc as the anion. They reveal the important role of X-groups in determining the selectivity and rate of elimination-limited reactions. The sample structures in Figure 2.6 illustrate that there is little direct interaction between the substrate and ligand. Instead, the temporarily displaced X-group lies between the two in a pocket lined by –CH groups of sparteine and the alcohol's methyl

group. We believe that the role of the anion at this point in the mechanism is to communicate steric interactions between ligand and substrate, while not covalently bound but held in place by electrostatic forces. The $C_{sparteine}$-Pd-C_{methyl} angle θ shown in Figure 2.6 increases from 135° in $\mathbf{21}^{\ddagger}$ to 139° in $\mathbf{18}^{\ddagger}$ to 146° in $\mathbf{9}^{\ddagger}$ to accomodate the counterions. By filling the space between the methyl group and ligand differently, the two anions present the same substrate with slightly different environments. The asymmetry of sparteine ensures that R and S alcohols face different combinations of steric interference as they pass through this transition state, hence the selectivity.

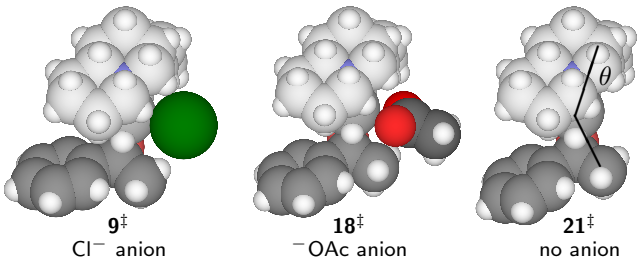

Figure 2.6: β-hydride elimination transition states incorporating chloride ($\mathbf{9}^{\ddagger}$), acetate ($\mathbf{18}^{\ddagger}$), and no anion ($\mathbf{21}^{\ddagger}$), optimized in toluene. The anion nestles between the ligand and substrate, increasing the $C_{sparteine}$-Pd-C_{methyl} angle θ.

To validate the role of these diastereomeric transition state structures their energies were used to predict enantioselectivities ($\mathbf{s}_{calc}$) of reactions limited by β-hydride elimination using the method of the following section. A selectivity factor of $\mathbf{s}_{calc} = 17.7$ is calculated for 1-phenylethanol in toluene at 60°C when X = Cl^-, and $\mathbf{s}_{calc} = 7.4$ at 80°C in toluene and $\mathbf{s}_{calc} = 14.9$ at 60°C in 1,2-dichloroethane when X = $^-$OAc. Bagdanoff et al. [39] report $\mathbf{s}_{exp} = 20.0$ at 60°C using (norbornadiene)$PdCl_2$ as a palladium source. (This datum is interpreted here as representing the β-hydride elimination-controlled regime because of the excess base, Cs_2CO_3, present.) Starting with $Pd(OAc)_2$, Ferreira and Stoltz [31] report $\mathbf{s}_{exp} = 8.8$ at 80°C in toluene and Jensen et al. [32] report $\mathbf{s}_{exp} = 13.0$ at 60°C in dichloroethane.

To further emphasize the anion's role in the β-hydride elimination step, transition states were found for (R)- and (S)-1-phenylethanol with no anion present. The separation of charge implied by removing the anion from the resulting cationic complex (e.g. $\mathbf{21}^{\ddagger}$ in Figure 2.6) is energetically unrealistic in a low-dielectric medium such as toluene. Higher elimination barriers ($\Delta E^{\ddagger}_{sol} = 36.4$

kcal/mol relative to reactants) are predicted when Cl^- is solvated separately than when Cl^- is allowed to remain close to the reaction center. More striking is that practically no discrimination between enantiomers is predicted ($\mathbf{s}_{\text{calc}} = 1.5$), suggesting no selectivity would be observed if the anion were not present between the ligand and substrate to amplify it.

2.4 Selectivity

2.4.1 General

The enantioselectivity displayed by a catalyst/substrate pair is a convolution of the relative rates of the coordination (e.g. **1**→**7**), deprotonation (**7**→**8**) and β-hydride elimination (**8**→**10**) events. An algebraic expression for selectivity in terms of these rates (k_{Coord}, k_{DP}, $k_{\beta\text{HE}}$) and their associated equilibrium constants depends on one's choice of rate law and the conditions employed in the reaction and cannot be written down *a priori*. We find that selectivities observed in kinetic resolutions of racemic mixtures under base-rich conditions are accurately described by

$$\mathbf{s}_{\text{calc}} = \frac{\text{rate}_R}{\text{rate}_S} = \frac{\sum_R A_o exp(-\frac{\Delta E^{\ddagger}_{\text{sol}}}{RT})}{\sum_S A_o exp(-\frac{\Delta E^{\ddagger}_{\text{sol}}}{RT})} \tag{2.1}$$

when $\Delta E^{\ddagger}_{\text{sol}}$ is the calculated energy of a βHE transition state relative to the reactants (Figure 2.7). Since the asymmetry of sparteine makes the two sites occupied by Cl atoms in the resting state incongruent, two βHE transition states exist for each enantiomer. Distinguished by which Cl atom is initially displaced by the alcohol, we consider these two structures (e.g. R1 and R2 or S1 and S2 in Table 2.1) to belong to separate reaction pathways. (Four additional isomers, analogues of R1-S2, can be generated by swapping the methyl and aryl groups of the substrate so that the anion resides adjacent the aryl group instead of the methyl group. For 1-phenylethanol, the unfavorable interaction of the anion with the π-electrons of the aryl group causes the energies of these isomers to lie $2\frac{1}{2}$ to 4 kcal/mol above their analogues R1-S2, and these isomers were subsequently ignored.) Hence the sums in Equation 2.1 contain two terms per enantiomer. Equal prefactors A_o are assumed.

By the same reasoning, experimental and calculated selectivities can be transformed into effective $\Delta\Delta G^{\ddagger}$'s (a measure of the degree to which a catalyst distinguishes between enantiomers) for a substrate/anion/solvent combination according to $\Delta\Delta G^{\ddagger}_{\text{eff}} = RT ln(\mathbf{s})$. Using only sparteine as a ligand, Jensen et al. found that the selectivity between (R) and (S)-1-phenylethanol ranged from 2.6 to 17.5 depending on their palladium source and reaction conditions [32]. Though the models only contain information regarding the substrate, X-group, solvent and temperature, they are able to consistently reproduce the selectivities observed in elimination-limited reactions.

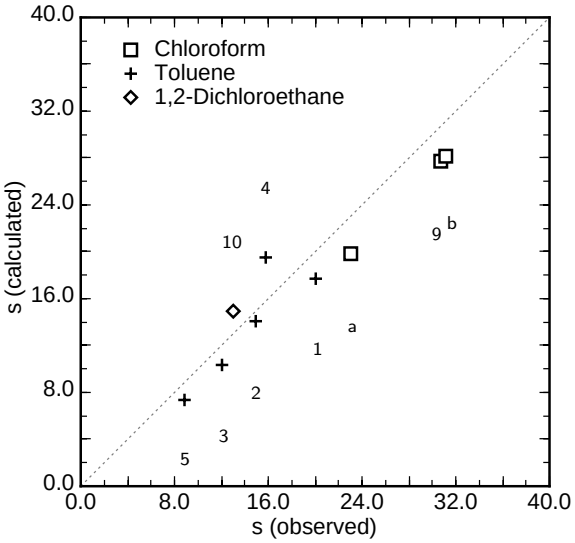

Figure 2.7: Calculated and experimental enantioselectivities. Labels denote corresponding entry in Table 2.1; a and b correspond to 1-(p-FC_6H_4)-ethanol and 1-(2-napthyl)-ethanol, respectively, in chloroform at 23°C, X = Cl^-.

Equation 2.1 is consistent with an expression such as

$$\mathbf{s} = \frac{K_{\text{Coord,R}} K_{\text{DP,R}} k_{\beta\text{HE,R}}}{K_{\text{Coord,S}} K_{\text{DP,S}} k_{\beta\text{HE,S}}}$$

in which all steps prior to βHE reach pre-equilibrium. Expressions derived from more complex mechanisms cannot, however, be excluded. The selectivity observed in the DP-limited regime differs from that in βHE-limited reactions for a given catalyst and is likely described by $\mathbf{s} =$

$K_{Coord,R}k_{DP,R}/K_{Coord,S}k_{DP,S}$. We focus on selectivity in the βHE-limited regime for two reasons. Barring a change in mechanism, new catalysts will achieve their highest rates under these conditions. Also, the βHE step may be more amenable to tuning with new ligands than deprotonation. An experimental combinatorial study [53] found that Pd complexes of both chiral and achiral ligands yielded functioning catalysts in the presence of sparteine (acting only as a chiral deprotonating agent). Unfortunately, selectivities resulting from these asymmetric deprotonations were not improved over sparteine-Pd complexes operating in the βHE-limited regime.

Four βHE transition states were located for a sampling of substrates (1-substituted ethanols), solvents and X-groups. The energetic and structural data collected in Table 2.1 show that configurations R1 and S2 provide the lowest-energy routes to the (R) and (S) substrates, respectively, though none of the four paths is negligible. We find the relative energies of the isomers are determined by three factors. First, transition state energies are lower if the anion is displaced to the open face of the ligand (below Pd in Table 1) than if it moves to the occluded face (above Pd). The rightmost piperidine ring of sparteine (as drawn) disrupts the coordination sphere of Pd by interfering with both the adjacent equitorial site (e.g. the adjacent chlorine in **1** is bent out of the square plane) and upper axial site (e.g. the anion in structure S1). Whether the oxygen of the substrate bonds to the left or right site on Pd is another factor. In the favorable site (R1, S1), oxygen abuts the less obtrusive, leftmost piperidine ring. This effect is most clearly seen in entry 6, in which no anion is present to otherwise affect the relative energies. Third, as mentioned, displacing the anion toward the aryl group of the substrate requires more energy than displacing it toward the methyl group. By combining the favorable aspects of each of these factors, structure R1 provides (R) substrates with the fastest oxidation pathway.

Selectivity predictions based on the combination of *gas phase* optimized transition state energies and single-point solvation energies only qualitatively matched the experimental observations. In particular, this approach failed to capture the high selectivities observed when chloroform is used as solvent. This suggested that solvent-induced geometric relaxation plays a significant role in addition to electronic relaxation. Therefore, all structures R1 through S2 were optimized *within* the

Table 2.1: Energetic and structural data of diastereomeric β-hydride elimination transition states

	Substrate / Anion	Solvent / Temp	E_{sol}[1] ($\Delta E^{\ddagger}_{sol}$[2]), kcal/mol C–$H_\beta$ (Å)	Pd···X[4] (Å)	E_{sol} C–H_β	Pd···X	E_{sol} C–H_β	Pd···X	E_{sol} C–H_β	Pd···X	s_{calc}[3]($\Delta\Delta G_{eff}$) s_{exp}[5]($\Delta\Delta G_{eff}$)
	bidentate sparteine		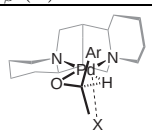 R1		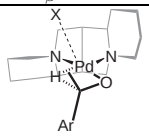 R2		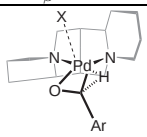 S1		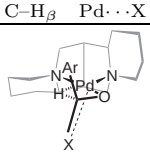 S2		
1	Ar = C_6H_5 X = Cl^-	toluene 60°C	0.0 (17.5) 1.61	3.11	1.73 1.64	3.23	2.82 1.52	3.11	2.03 1.62	3.28	17.7 (1.9 kcal) 20.0[6] (2.0)
2	Ar = *p*-$MeOC_6H_4$ X = Cl^-	toluene 60°C	0.0 (16.6) 1.58	3.25	1.21 1.61	3.28	2.65 1.48	3.12	1.82 1.59	3.31	14.1 (1.8) 14.9[6] (1.8)
3	Ar = *p*-FC_6H_4 X = Cl^-	toluene 60°C	0.0 (17.8) 1.61	3.24	1.18 1.64	3.23	2.36 1.53	3.11	1.63 1.62	3.31	10.3 (1.5) 12.1[6] (1.6)
4	Ar = 2-Naphthyl X = Cl^-	toluene 60°C	0.0 (15.7) 1.59	3.11	2.28 1.64	3.23	2.87 1.52	3.11	2.13 1.62	3.29	19.5 (2.0) 15.8[6] (1.8)
5	Ar = C_6H_5 X = ^-OAc	toluene 80°C	0.0 (24.1) 1.64	2.83	2.38 1.65	2.84	2.85 1.59	2.65	1.47 1.66	2.90	7.4 (1.4) 8.8[7] (1.5)
6	Ar = C_6H_5 None	toluene 60°C	0.0 (—) 1.50	—	1.55 1.55	—	0.28 1.50	—	1.54 1.55	—	1.5 (0.3) NA
7	Ar = C_6H_5 X = I^-	toluene 60°C	0.0 (14.5) 1.56	3.42	1.72 1.61	3.82	2.48 1.53	3.93	2.04 1.61	3.64	15.5 (1.8) NA
8	Ar = C_6H_5 X = Cl^-	vacuum 60°C	0.0 (23.4) 1.56	3.00	1.54 1.62	3.09	3.55 1.50	3.01	1.64 1.60	3.07	12.5 (1.7) NA
9	Ar = C_6H_5 X = Cl^-	CCl_3H 23°C	0.0 (14.6) 1.62	3.22	2.34 1.67	3.32	2.85 1.56	3.23	2.08 1.64	3.31	27.7 (2.0) 30.7[8] (2.0)
10	Ar = C_6H_5 X = ^-OAc	1,2-DCE 60°C	0.0 (26.5) 1.64	3.05	3.21 1.66	3.00	2.45 1.58	3.21	2.08 1.66	3.00	14.9 (1.8) 13.0[9] (1.7)
	monodentate sparteine		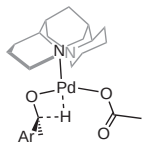 R3		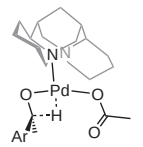 R4		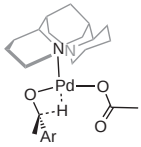 S3		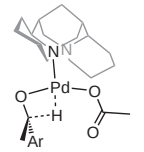 S4		
11	Ar = C_6H_5 X = ^-OAc	toluene 60°C	0.60 (24.7) 1.58	2.08	0.07 1.58	2.08	1.23 1.61	2.09	0.0 1.60	2.08	1.1 (0.1) NA

[1]Relative to lowest-energy isomer [2]Activation energy relative to reactants [3]From Equation 2.1 [4]When X = ^-OAc, distance to nearest O atom [5]Data best representing elimination-determined selectivities (i.e. base-rich reaction conditions) is used for comparison. [6]From reference [39] [7]From reference [31] [8]From reference [40] [9]From reference [32]

continuum solvent model, allowing the geometries and relative energies to more accurately reflect the action of the particular solvent.

2.4.2 Solvent Effects

Many organic solvents have proved competent for kinetic resolutions using sparteine-$PdCl_2$, with reactions in halomethanes excelling in both rate and selectivity[40]. Although the advantages associated with different solvents may also concern solubilities and the oxidation of the Pd-hydride intermediate, the effect of the dielectric on the βHE step is revealed by the evolution of the transition states in the different virtual solvents. The β-hydrogen displaces the remaining anion from its site as

the C-H_β bond breaks. Since breaking the polar Pd-X bond requires further separation of charge between the positively charged Pd center and the anion, it follows that a medium of increased dielectric strength should facilitate the process. The activation energies calculated for (*R*)-1-phenylethanol (traversing state R1, X = Cl^-) in vacuum, toluene (ϵ = 2.4) and chloroform (ϵ = 4.8) are 23.4, 17.5, and 14.6 kcal/mol, respectively. We find this trend to be general of all substrates. (When X = $^-$OAc, the predicted activation energies increase with the dielectric constant, but the sparteine-HOAc byproduct is responsible for reversal of this trend. Unlike the sparteine-H^+Cl^- complex, the acetic acid complex formed during the deprotonation of the bound alcohol is not polar enough to generate a large solvation energy. Consequently, reactants (**16**) are favored over later intermediates as the dielectric increases. However, the energy difference between the *alkoxide* and βHE states is decreased by increasing dielectric strength whether X = Cl^- or $^-$OAc.) That the solvent is stabilizing the charge separation is manifest in the increasing Mulliken population of the Cl^- ion: -0.65 $|e^-|$ in vacuum, -0.74 $|e^-|$ in toluene, and -0.79 $|e^-|$ in chloroform (structures R1 of entries 8, 1 and 9).

The increase in reaction rate observed in chloroform (relative to toluene) is apparently also the primary factor responsible for the observed increase in selectivity. A facile kinetic resolution can be performed at lower temperatures, where a catalyst's discrimination between enantiomers (i.e., $\Delta\Delta G^{\ddagger}_{eff}$) leads to a higher selectivity factor. For example, Bagdanoff, using a dichloride catalyst and 1-phenylethanol, reported a selectivity of 20.0 in toluene [39] at 60°C and 31 in chloroform [40] at 23°C, suggesting the same $\Delta\Delta G^{\ddagger}_{eff}$ of 2.0 kcal/mol in each solvent. However, a second mechanism is also at work, by which the solvent influences $\Delta\Delta G^{\ddagger}_{eff}$'s directly. 1-(*p*-fluoro)-phenylethanol exhibited a selectivity of 12.1 at 60°C in toluene [39] and 23 at 23°C in chloroform [40], yielding disparate $\Delta\Delta G^{\ddagger}_{eff}$'s of 1.65 and 1.84 kcal/mol, respectively. (Both increases and decreases in $\Delta\Delta G^{\ddagger}_{eff}$ are observed among the substrates.) Though possibly due to a difference in the activation entropies of enantiomers, this more subtle effect may also be mediated by the response of the displaced anion to more polar solvents. Two trends regarding the anion are clear in the calculations. One is the aforementioned accumulation of charge allowed by higher dielectrics. The second is the increase

in the Pd$\cdots$X distance in transition states optimized in more polarizable media. (See Entries 8, 1 and 9, or 5 and 10). In stabilizing the forming dipole the solvent draws the charged species further into solution. Together these two effects allow the solvent to influence the effective size and position of the X-group. Since the X-group is responsible for communicating steric interactions from ligand to substrate, it follows that the solvent's influence should extend to the discrimination between enantiomers. An additional selectivity prediction using dichloromethane as solvent (for 1-phenylethanol at 60°C, X = Cl^-, ϵ = 9.1) yielded $\mathbf{s}_{\mathrm{calc}}$ = 13.1. The βHE structures relaxed in this dielectric show that the chloride ion moves still farther from the palladium center, and this is likely the cause of the decrease in calculated selectivity from chloroform to dichloromethane. We propose that there is a critical dielectric constant above which (with the help of entropy) the anion would be solvated entirely separate from the cationic complex. For example, using a dielectric of 80.4 to represent water we find the separate ions Cl^- and $\mathbf{21}^{\ddagger}$ have a slightly *lower* energy than the complex $\mathbf{9}^{\ddagger}$. Were the reactants still soluble in so polar a medium, enantioselectivity would be lost.

2.4.3 Substrates and Anions

The oxidation rates of substituted benzylic alcohols in the presence of excess sparteine were observed to increase with the electron-donating strength of the substituent [38]. This was attributed to a rate-limiting βHE step in which negative charge is drawn from the alkoxide to the resulting Pd-hydride complex. Our calculations involving para-substituted 1-phenylethanols (Entries 1-3) show the same behavior; that is, the activation energies $\Delta E^{\ddagger}_{\mathrm{sol}}$ increase with the Hammett parameters of the substrates. In accordance with the Hammond Postulate, we find that transition state structures of less easily oxidized substrates are more product-like. For example, the C-H_β bond being broken in each transition state incorporating 1-(*p*-fluoro)-phenylethanol is at least 0.03 Å longer than the corresponding C-H_β bond in 1-(*p*-methoxy)-phenylethanol.

To explore the properties of other counterions, chlorine was replaced with iodine in the model reaction and the key energetics calculated. The predicted selectivity ($\mathbf{s}_{\mathrm{calc}}$= 15.5 at 60°C, entry 7) is no greater than that of the dichloride catalyst, but the activation energy of the lowest βHE transition state ($\Delta E^{\ddagger}_{\mathrm{sol,I,R1}}$ = 14.5 kcal/mol) is lower (cf $\Delta E^{\ddagger}_{\mathrm{sol,Cl,R1}}$ = 17.5). This reflects the ground-state

destabilization of the initial (sparteine)PdI_2 complex; the crowding of sparteine and the large iodine atoms around Pd effectively weakens the Pd-X bonds which must be broken during the cycle. High activity can be translated into higher selectivity by operating at a lower temperature, as noted.

When X = $^-$OAc, βHE transition states incorporating monodentate sparteine (entry 11) are as energetically accessible as those with the ligand chelated (entry 5). In this geometry the ligand dominates the coordination sphere even less than when bidentate, and the variation in energy among the isomers (and hence the predicted selectivity) is correspondingly small. Still another group of isomers exists in which the oxygen of the substrate bonds trans to monodentate sparteine, but the activation energies associated with this geometry are 8 kcal/mol higher than the structures shown.

2.4.4 Thermodynamics

The discussion above relies on solution phase energies rather than enthalpies or free energies. Accurate gas phase thermodynamic properties for the various intermediates can be calculated by applying the appropriate formulas of statistical mechanics to frequency spectra derived from calculated (gas phase) hessians. Solution phase enthalpies are accessible from the gas phase values by subtracting PV and including the calculated solvation energies. This assumes the six hindered translational and rotational modes still behave classically and contribute $\frac{6}{2}$kT to the total energy and the vibrational frequencies do not change appreciably in solution. In this manner solution phase enthalpies H_{sol} at 298K were calculated for the model reaction. This yielded: reactants (**1**), 0.0 kcal/mol; substitution transition state (**6**‡), 5.2; alcohol complex (**7**), -1.1; alkoxide complex (**8**), 1.3; and βHE transition state (**9**‡), 16.2. (The last value can be compared to the activation enthalpy of 16.8 kcal/mol measured by Mueller and Sigman [38] in 1,2-dichloroethane using an Eyring plot from 30 to 65°C.) Since the "reactants" state is composed of three separate molecules (alcohol, sparteine-$PdCl_2$, and free sparteine) and subsequent stages of the oxidation involve only two (Pd-substrate complex and sparteine-H^+Cl^- complex), the *free energy* of the reactants will be even lower relative to the other intermediates because of their greater entropy. This explains the observation of a first-order dependence of reaction rate on substrate concentration under all conditions. As long as the reactants are lowest in free energy, increased alcohol concentration will drive more palladium from state **1** to

states **7** and onward.

The relative solution phase *enthalpies* of the βHE transition states incorporating 1-phenylethanol and chloride (entry 1) are 0.0 (R1), 1.7 (R2), 2.8 (S1) and 2.1 (S2). In general, we find that selectivity predictions based on solution phase enthalpies yield qualitatively similar results to those based on energies but with more variation from the experimental measurements. The gas phase entropies of the same four species are within 1 eu of one another, and for other substrates the variation is less than 5 eu. Therefore we conlclude that energy (or enthalpy) differences alone are sufficient to explain enantioselectivities derived from βHE. Thus we rely on solution phase energies, reaching the same conclusions and avoiding the assumptions associated with gas phase hessians.

2.4.5 Other Approaches

Our work joins a number of increasingly quantitative calculations of the outcome of stereoselective reactions in solution and in proteins. Many algorithms have been applied to this problem, employing a variety of methods for the evaluation of energies (forcefields [54], DFT [55], empirical correlations [56]) and structural models (explicit transition states or more abstract concepts [57]). Some factors which aid the reliability of predictions, however, are recurrent. Relative reaction rates often result from a flux of chiral or prochiral molecules through not just two transition states (e.g. (R) and (S)), but through a collection of diastereomeric states. A computational model should reflect this by averaging over an ensemble of all thermodynamically relevant reaction paths. Also, variations in the solvent-accessible surface of these isomeric transition states can contribute to or even determine selectivity [56]. A model of solvation is therefore helpful or necessary, depending upon the reaction in question.

2.5 Conclusions

The mechanism for oxidation of *sec*-alcohols by ((–)-sparteine)PdX_2 compounds begins with the facile substitution of an alcohol for an anion, followed by the deprotonation of the bound alcohol. Chloride is too weak a base to drive this step alone and requires free sparteine or a basic additive to form a Pd-alkoxide. Acetate and stronger bases can perform the deprotonation alone or in

conjunction with sparteine at rates dependent on their basicity and concentration.

Once the ensuing β-hydride elimination step becomes rate-limiting, the enantioselectivity displayed by a catalyst in the presence of a racemic substrate is a function of the relative energies of an ensemble of diastereomeric βHE transition state structures. The anion plays a critical role in these transition states by mediating the interaction between the otherwise estranged ligand and substrate. Solvents influence rate and selectivity during the elimination by accomodating an increase in charge on the anion. In addition to aiding the interpretation of existing results, the ability to compute activation energies and enantioselectivities provides a tool for screening new catalyst/substrate combinations.

Chapter 3

New Ligands for Enantioselective Oxidations: Sparteine Mimics

The motivation for searching out ligands which could replace (–)-sparteine in palladium-mediated enantioselective oxidations is not simply to test the current efficacy of computation-based design strategies. Despite the success of the (–)-sparteine/Pd^{II} protocols in resolving benzylic and allylic alcohols, they leave their employers wanting for some complimentary capabilities. Only complex synthetic routes to (+)-sparteine exist([58, 59] and references therein), while its antipode is still in practice obtained from the natural botanical source. Since (+)-sparteine is therefore unavailable, kinetic resolutions of racemic *sec*-alcohols are limited to yielding only one of the two enantiomers. The ligand's natural production and saturated hydrocarbon framework also discourage any modification of its structure (e.g., to optimize its interaction with new substrates or to alter its solubility). Finally, non-selective palladium catalysts (see Chapter 4) are known to oxidize alcohols faster, perform in water, or react with a broader slate of substrates (primary and saturated alcohols). Any of these traits would be desirable in a new catalyst.

Ligands too numerous and complex to study individually have already proved less effective than sparteine in kinetic resolutions of *sec*-alcohols. However their structures and comparisons of the experimental and theoretical observations allow speculation regarding which motifs may be responsible for reaction rates and selectivities in current and future catalysts.

The ligands in group (a) (Figure 3.1) each yielded higher rates than sparteine in the $Pd(OAc)_2$-catalyzed oxidation of 1-phenylethanol under similar conditions[31, 32]. Their enantioselectivities,

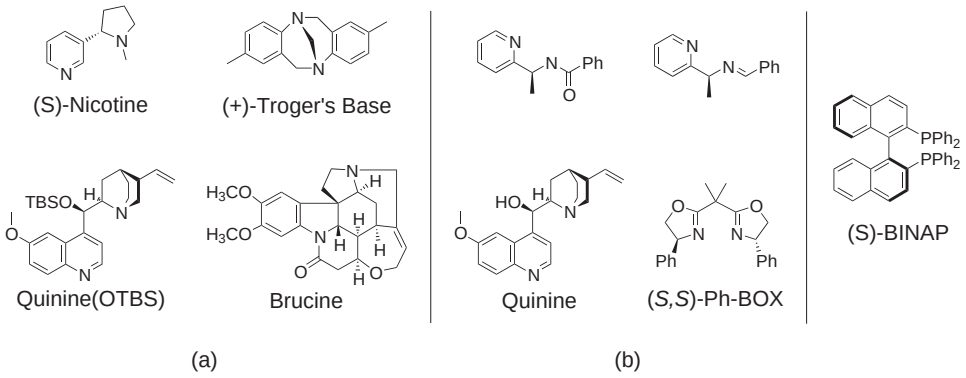

Figure 3.1: A sampling of ligands from the screens[31, 32] that identified (–)-sparteine as an effective ligand.

however, were unobservable or small. Members of this group have either sp^3 or both sp^3 and sp^2 N-atom lone pairs available for bonding to Pd (neglecting oxygen atoms). The geometries of all four dictate that they bond to Pd through only one N at a time. Members of group (b) and others displayed no selectivity and lower rates than sparteine when tested. Possibly multidentate, these ligands provide either sp^2 or both sp^2 and sp^3 N lone pairs. The chiral phosphine BINAP also showed rates similar to sparteine and no enantioselectivity.

Sparteine's rigid structure forces it to chelate in a cis, bidentate fashion, while L_2PdX_2-type compounds generally prefer a trans arrangement. If, for monodentate ligands, the alkoxide requires two of the four Pd sites during β-hydride elimination (βHE), then the lowest-energy transition structure will have either the form LXPd(alkoxide) or L_2Pd(alkoxide). The former case is likey unselective for other ligands, as it is for sparteine (see Table 2.1). The latter case, which would require extra mechanistic steps to rearrange the ligands from a trans configuration, may be energetically inaccessible from the (more stable) trans resting state (Figure 3.2). So it would seem only a catalyst with a cis resting state can lead to an accessible *and* selective βHE transition state.

Group (a) ligands are interpreted to form monodentate $(\text{ligand})_2PdX_2$ complexes which pass quickly through the unselective βHE transition state in Figure 3.2. The rotational flexibility in the backbones of the group (b) ligands leaves it uncertain whether they are chelated in the resting state of the catalyst or acting as unselective monodentate ligands. Even if they are chelated, their lack of selectivity can be rationalized by comparing their shape to (–)-sparteine's. The nitrogen lone pairs

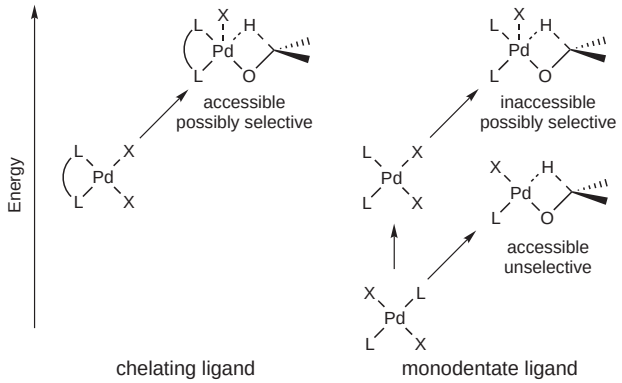

Figure 3.2: Interpretation of chelating and monodentate ligands' reactivity.

used to bind palladium to (–)-sparteine are buried in a chiral pocket formed by the surrounding piperidine rings. Its bulk notwithstanding, this ligand still needs the assistance of the associated anion to exert its enantiospecificity on the bound substrate. The lone pairs of other ligands (with the exception of the bis-oxazoline (*S,S*)-Ph-BOX) protrude from a chiral environment, permitting the ligand to dominate even less of the coordination sphere.

In light of this, we expect a successful (–)-sparteine mimic will prefer chelation during each step of the catalytic cycle. Its structure must not only be asymmetric, but its asymmetry must be projected toward the metal and substrate. Tertiary amines are associated with the fastest oxidations and foster bulky environments, but sp^2 nitrogen donors are also well represented among reported oxidation catalysts.

3.1 Search Strategy

3.1.1 Computational Assays

The first attempt to identify a synthetic sparteine surrogate relied on the notion that any difference between a proposed catalyst system and the established (–)-sparteine-based protocol would invite new mechanisms for catalyst deactivation, unselective reaction, or other undesirable side-effects which would take time to understand and alleviate. Therefore, a catalyst as similar to ((–)-sparteine)PdX_2 as possible, which would follow the same mechanism, was sought. Recall that the conditions under which the (–)-sparteine catalyst was discovered employed free (–)-sparteine

molecules in solution to deprotonate the alcohol (in a potentially enantioselective step) after the alcohol had joined the metal-ligand complex[38]. Later it was discovered that inorganic bases such as Cs_2CO_3 were effective deprotonating agents[39] and enantiodescrimination could be achieved during the β-hydride elimination. We accordingly planned to employ a similar exogenous base for the deprotonation and optimize a new ligand to provide enantioselectivity solely in the βHE step. Specifically, proposed ligands were computationally screened for:

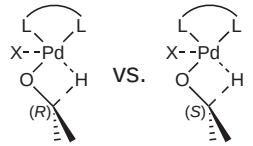

Selectivity ($\mathbf{s}_{\mathrm{calc}}$)

Using what was learned of the ((−)-sparteine)PdX_2 catalyst (i.e., that under base-rich conditions which maximize the reaction rate selectivity is determined by the disparity between β-hydride elimination activation barriers encountered by (R) and (S) alcohols, and that the anion plays a crucial role in the βHE transition states) Equation 2.1 was used to predict ligands' potential enantioselectivity (in reactions with 1-phenylethanol in toluene at 60°C. To expedite screening, transition state geometries were located in the gas phase and subjected to single-point (no-relaxation) solvation calculations in toluene. Simulations using (−)-sparteine showed that accurate prediction of selectivities requires transition states to be optimized withing the solvent model, while the faster approach could err by a factor of 2. This level of estimation was still sufficient to identify candidates worthy of further attention. The number of necessary diasteriomers contributing to the sums in Equation 2.1 was considered on a case-by-case basis. A rigorously C_2-symmetric catalyst, for example, requires half as many calculations as a C_1 ligand like (−)-sparteine.

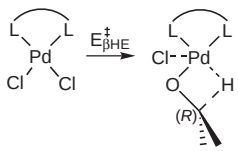

β-hydride elimination barrier ($\mathrm{E}^{\ddagger}_{\beta\mathrm{HE}}$)

The difference in energy (electronic plus solvation energy, with no zero-point energy correction) between the dichloride starting material and the βHE transition state (incorporating (R)-1-phenylethanol) was used as an indicator of reaction rate. This calculated quantity ranged from 16 to 24 kcal/mol for reactions of dichloride and diacetate complexes known to occur in toluene (see Table 2.1), so values in this range were considered favorable.

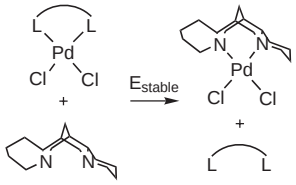

Stability (E_{stable})

The exothermicity of replacing the proposed ligand with (–)-sparteine was used to measure the relative stability of the L_2PdCl_2 complex (a positive value denotes improved stability). Known ((–)-sparteine)Pd complexes have not been found to suffer decomposition, so acceptable values for this parameter were not known *a priori*.

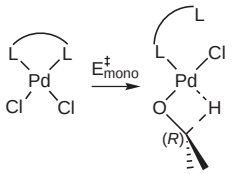

Unselective reaction ($E^{\ddagger}_{mono}$)

In studying the ((–)-sparteine)Pd$(OAc)_2$ catalyst it was found that βHE from a monodentate sparteine complex was energetically (if not kinetically) competitive with the enantioselective pathway. A ligand less rigid than (–)-sparteine might allow a flux of reactant through this non-selective mechanism.

3.1.2 Candidates

Tethered amines which can lose their tentative stereochemistry by a simple inversion of nitrogen centers (Figure 3.3, a and b) are not suitable scaffolds. Other known ligands have stereocenters locked into the carbon framework (e.g., c and d[1]), but their flexibility raises concerns that they will

[1] d and similar ligands designed by Beak, et al.[60] showed various enantioselectivities as replacements for (–)-sparteine in asymmetric lithiations.

not remain chelated throughout the reaction.

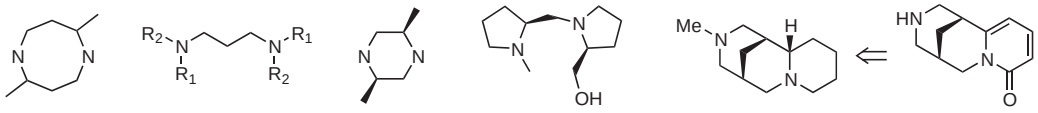

Figure 3.3: Asymmetric tethered amines.

Dearden et al.[61] sought to mimic (+)-sparteine with a synthetically tractable derivative of (–)-cytisine, (+)-e. Though the ligand successfully catalyzed several asymmetric lithiations with enantioselectivity similar (but opposite) to (–)-sparteine, the kinetic resolution of 1-indanol yielded a s_{exp} of 3.9[2], half that of (–)-sparteine[31]. We investigated the reaction of 1-phenylethanol with the $PdCl_2$ complexes of (–)-e and the *t*-butyl derivative (–)-f (Figure 3.4). That the stability of these ligands decreases with the bulk of the N-substituent is reflected in the distortion of the L_2PdCl_2 geometries (note the N-Pd bond lengths). Though βHE activation energies were acceptable in the cases studied, enantioselectivities were low ((–)-e) or negligible ((–)-f). The low $\Delta E^{\ddagger}_{\beta HE}$ in the case of (–)-f (12 kcal/mol) reflects a ground state destabilization more than a facile beta hydride elimination. The strain induced by the bulky *t*-butyl group, which raises the energy of the dichloride complex, may cause the subsequent L_2PdCl(alcohol) or L_2PdCl(alkoxide) species to become the catalyst's resting state[3].

[2]This level of discrimination is interesting academically, but the resolved product is not of useful enantiopurity (80% ee at 76% conversion).

[3]Or, more likely, the complex would simply not form.

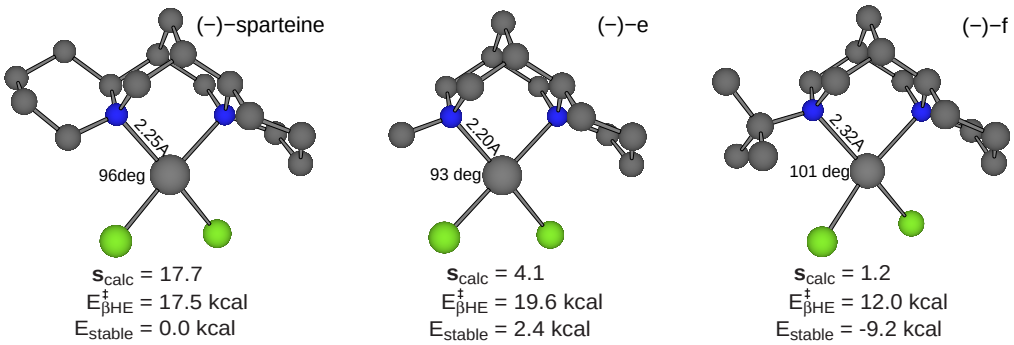

Figure 3.4: Characterization of (−)-cytisine derivatives. L_2PdCl_2 complexes are shown with N-Pd bond lengths and N-Pd-Cl bond angles noted. $\mathbf{s}_{calc}$ of (−)-e was based on only one (R) and one (S) diastereomer.

While the adaptation of (−)-cytisine allows some room for tuning, initial results were discouraging and syntheses still start from the natural product, obtained from ground *Laburnum anagyroides* seeds[62, 63]. A more promising class of tunable, rigid, diamine scaffolds are the bispidinones and bispidines (Figure 3.5). The fused bicyclic core of sparteine is preserved in these molecules, while the asymmetric outer rings are lost. These ligands have been shown to bind to several metals, including Pd^{II}. Bispidinones self-assemble from common starting materials in moderate yields[64], and the synthesis of bispidines is not prohibitive[65]. We reasoned that by incorporating optically active primary amines into these syntheses, a C_2-symmetric pocket would be constructed around the guest metal atom. Enantioselective reactions would depend on the integrity of this pocket, which could be ruined by rotation around the N-C* bond (a degree of freedom not present in sparteine). We hypothesized that if one of the substituents on the stereocenter was chosen to be much larger than the others, its steric bulk would force the chiral arms of the ligand to always adopt the same configuration during βHE. In fact the ligand (*S,S*)-**g**, incorporating (*S*)-1-phenyl-ethylamine, had been synthesized and incorporated in a cationic Pd^{II}-allyl complex[65]. Encouragingly, 2D-NMR showed that, at low temperature, the phenyl group did act as a "molecular brake", forbidding rotation about the N-C* bond.

The next section decribes our investigation of this class of ligands, followed by the experimental observations made in the Stoltz lab at Caltech.

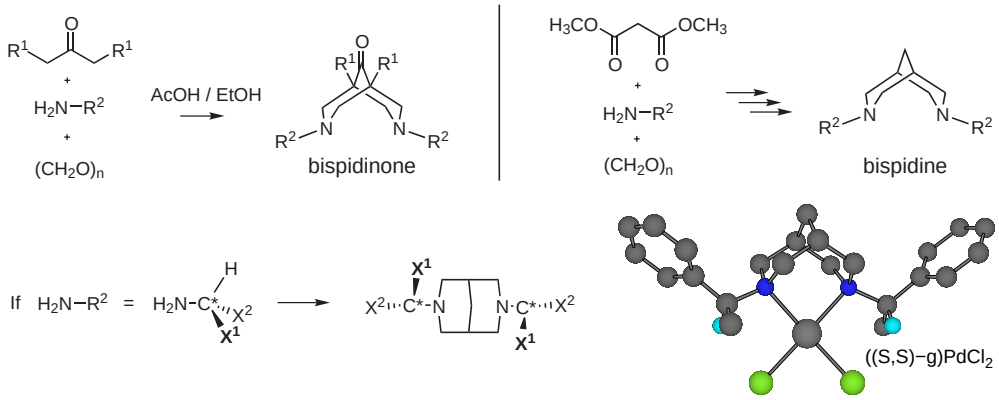

Figure 3.5: Structure of bispidinones and bispidines. Hydrogens on the stereocenters are light blue.

3.2 Theoretical Results

The number of available chiral primary amines permits many variations on the bispidine structure to be imagined. Candidates for modeling were chosen to provide a range of steric and electronic properties. Of the three substituents on the carbon stereocenter, one was always chosen to be hydrogen. First, this ensured that two quadrants of the space around the palladium atom would be relatively free to accomodate the combined bulk of the anion and substrate during βHE. Second, it became apparent that if all three substituents on the stereocenter were larger than hydrogen, insufficient space was left for other groups bound to palladium. Recall the instability of ligand f in Figure 3.4.

The ketone moiety in the backbone of the bispidinones, though separated from the nitrogen lone pairs by several bonds, significantly affects the strength with which these ligands bind palladium. The bispidinone j, 11.1 kcal/mol less stable than sparteine, becomes more robust when its backbone is saturated to make the bispidine g, only 6.4 kcal/mol less stable than sparteine (Figure 3.6). The ability of the nitrogen lone pairs to provide charge for the dative bonds to palladium is further reduced when the methyl substituents are replaced by trifluoromethyl groups (i). The electron-deficiency of a ligand is also manifest, beneficially, in the βHE activation energy associated with it. It was shown by ten Brink et al. that electron withdrawing substituents on their bipyridine-derived ligands promoted alcohol oxidation rates[66], consistent with the oxidative nature of the rate-limiting β-hydride elimination. The same effect is observed here, as $E^{\ddagger}_{\beta HE}$ decreases from ligand

g (17.9 kcal/mol) to j (17.8 kcal/mol) to i (16.4 kcal/mol).

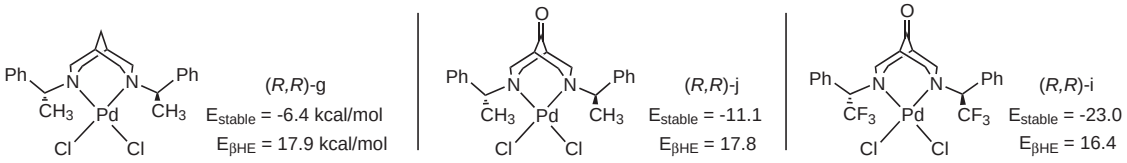

Figure 3.6: Stability and βHE activation energies of bispidine and bispidinone ligands.

Rotation around the N-C* bond is expected to have an activation barrier low enough that this degree of freedom occupies an equilibrium distribution during βHE events. For simplicity, the relative energies of the three staggered conformations of one of these bonds in L_2PdCl_2 complexes were evaluated (Figure 3.7). When the three substituents on the stereocenter are hydrogen, phenyl and trifluoromethyl (ligand i), two rotamers of the complex (a and b) are equally stable. Since in configuration b the hydrogen substituents of both stereocenters are on the same face of the palladium square plane, the environment around palladium is roughly of C_S symmetry. This environment is expected not to foster enantiomeric discrimination, so this configuration should be discouraged in a successful ligand. In configuration c, both the phenyl and trifluoromethyl groups interfere with the substituents on palladium, making this case consistently less stable. A fourth geometry, in which both chiral arms have rotated, was found to be 11.8 kcal/mol less stable than a. A *t*-butyl group was found to be less effective as a molecular brake than phenyl: in the case of ligand l, configuration b is most stable. In configuration a, the *t*-butyl groups abut the bispidinone framework and the charge-rich trifluoromethyl groups repel the chlorine atoms. Both of these offenses are relieved in configuration b. Ligand g behaves ideally: the C_2-symmetric configuration a is favored over the others by a margin large enough to preserve enantioselectivity.

More complete computational assays of three representative ligands are presented in Table 3.1. The βHE activation energies typical of the bispidine framework are fortunately similar to that calculated for sparteine. The electronic properties of the ligands influence this barrier as discussed, while the sterics by design interfere with the anions and substrate in a manner similar to sparteine. The cause for concern is the stability of these ligands. No catalyst which differs from sparteine by

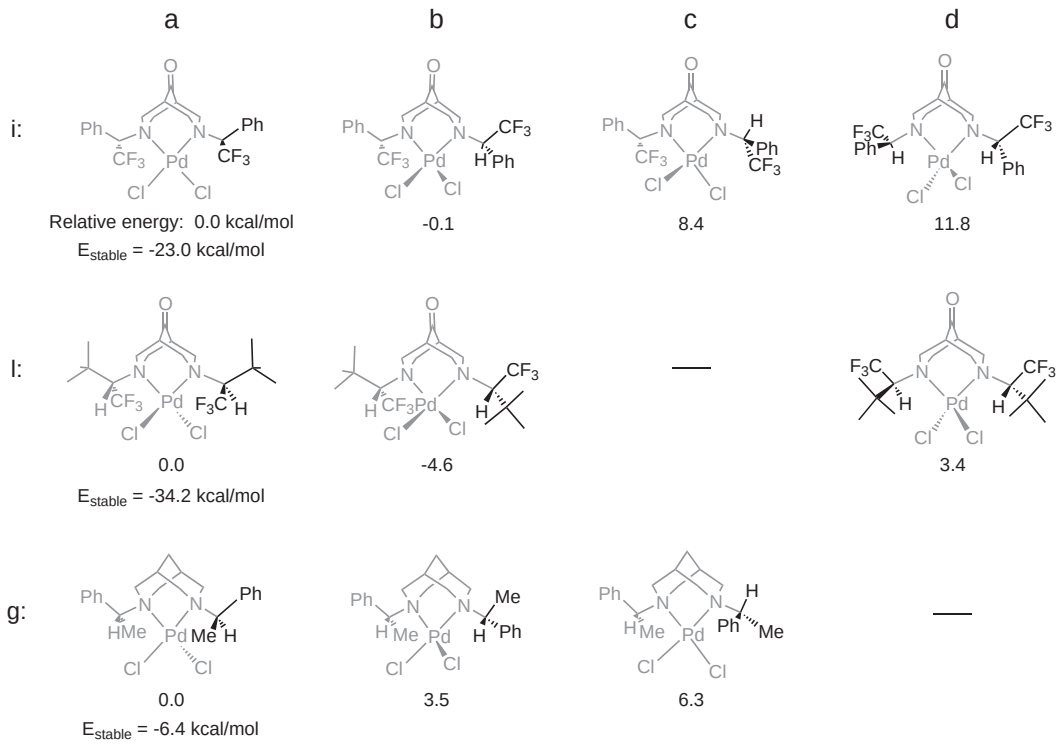

Figure 3.7: Relative solvated energies of rotamers of bispidine and bispidinone ligands. Energies are relative to configuration *a*, and E_{stable} corresponds to configuration *a*. Chlorine atoms are pushed out of the square plane by large adjacent groups.

more than 20 kcal/mol in any respect (i.e., E_{stable} for the fluorinated ligand i) can be assumed to follow the same mechanism. The possibility of unselective reaction is closely related to a ligand's stability since one of the Pd-N bonds must be broken during this alternative β-hydride elimination. Ligand i, not surprisingly, prefers the monodentate path to the bidentate path thermodynamically (though reactivity depends on the kinetics of this route as well[4]). We hoped, nonetheless, that the methyl and silyl derivatives g and h, only 6 to 8 kcal/mol less stable than sparteine, would still fall into the desired reaction manifold in the absence of competing ligands.

Most importantly, these ligands were predicted to be capable of matching the selectivity demonstrated by (−)-sparteine catalysts. The chiral arms of candidates g and h were calculated to prefer configuration a over b (see Figure 3.7) by over three kcal/mol, and in this geometry were predicted to display selectivity factors of 14 and 26, respectively, in kinetic resolutions of 1-phenylethanol.

[4]Recall that the ((−)-sparteine)$Pd(OAc)_2$ catalyst apparently follows the enantioselective mechanism despite the calculations showing the two routes to be isoenergetic.

Table 3.1: Computational evaluation of new bispidinone and bispidine ligands

Ligand	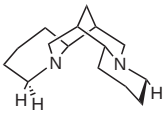 (–)-sparteine	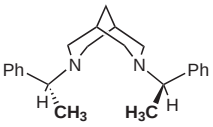 (*R*,*R*)-g	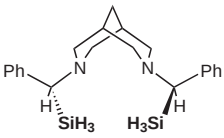 (*R*,*R*)-h	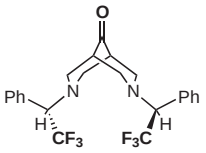 (*R*,*R*)-i
Activation energy[1] $E^{\ddagger}_{\beta HE}$	17.5	17.9	19.1	16.4
Selectivity[2] $\mathbf{s}_{calc}$	17.7	14.1	26.0	250
Stability E_{stable}	0.0	-6.4	-7.7	-22.9
Unselective reaction $E^{\ddagger}_{mono}$	22.5	19.4	—	11.0

[1] See section 3.1.1 for descriptions of computed parameters. All parameters take Cl^- as the anion. Energies in kcal/mol. [2] Selectivity factors here were derived from βHE transition states optimized in toluene.

The high selectivity factor of i (250 at 60°C) is unlikely to be observed due to ligand instability, but it illustrates an important new concept not yet exploited by the ligands experimentally or theoretically tested. The success of (–)-sparteine (and the failure of other ostensibly well-suited ligands) in descriminating between antipodes is based in *volume-exclusion*: the shape of the ligand/metal/anion complex at the time of βHE permits one substrate to assume its ideal geometry at the transition state while forcing its enantiomer into a slightly distorted geometry. In addition to this steric effect, *hydrogen bonding* interactions with ligands' -OH groups apparently direct other enantioselective reactions[67, 60]. Hydrogen bonding might be well applied in the current design problem to direct and stabilize the displaced anion during βHE. Care would have to be taken to protect any alcoholic group in a new ligand from being oxidized itself. Besides these short-ranged interactions, ligand i employs *electrostatic* forces to shape the geometry of the complex. During βHE from an (*R*) substrate, the anion neighboring the alkoxide is displaced from palladium to a position above the Pd-H_β bond. The electrostatic potential there is more favorable for an anion than above the Pd-O bond. During βHE from an (*S*) substrate, however, the -CH_3, -SiH_3, and -CF_3 groups adjacent the hydride in ligands g, h and i inhibit (to different degrees) the displaced anion from remaining over the Pd-H_β bond (Figure 3.8). Even though the -CF_3 group is smaller than the -SiH_3

group (by summing van der Waals radii), the chloride anion is repelled farther across the face of the square plane by the electron-rich trifluoromethyl group than by the silyl group. Since the anion is forced into a region of high potential energy, the (*S*) enantiomer must overcome an activation barrier 3.6 kcal/mol higher than the (*R*) enantiomer in the case of ligand i. *The long-range potential of electrostatic interactions may be useful in the design of ligands based on more stable scaffolds.*

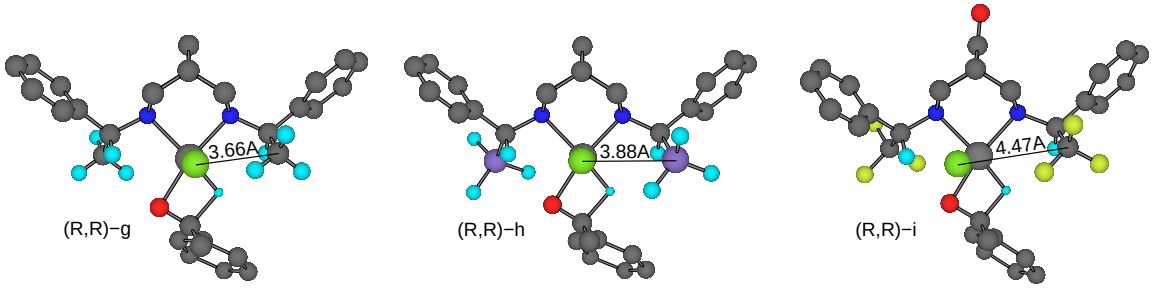

Figure 3.8: Transition states for beta-hydride elimination from (*S*)-1-phenylethanol for ligands g, h and i. The Cl···C or Cl···Si distance is noted.

3.3 Experimental Results

In light of the theoretical results, the group of Prof. Brian Stoltz synthesized and tested several bispidine and bispidinone ligands. My thanks go to Jeffrey Bagdanoff for his effort. Following the work of Rose et al. [64] (Figure 3.5), the molecules in Figure 3.9 were made, and ^{1}H NMR spectra showed the desired products were isolated. (For example, ligand k yielded Figure 3.10a.) Conversion in these reactions was higher for ligands which precipitated from solution. However, the attempts to metallate these ligands with $(H_3CCN)_2PdCl_2$ did not yield unique products. NMR spectra showed numerous peaks suggesting multiple products had formed (Figure 3.10b), and a unique ligand·Pd complex was not isolated. Furthermore, when the reaction mixture was applied to 1-(*p*-methoxyphenyl)ethanol under standard catalytic conditions[5], no oxidation products were observed. This contrasts the behavior of (−)-sparteine, with which kinetic resolutions are successful whether cystalline ((−)-sparteine)$PdCl_2$ is employed or the catalyst is generated in situ from free (−)-sparteine and any of a variety of palladium salts.

Follow-up calculations rationalize several unwanted complexes which may compete with the de-

[5] 80°C in $CHCl_3$, under 1 atm O_2, with Cs_2CO_3

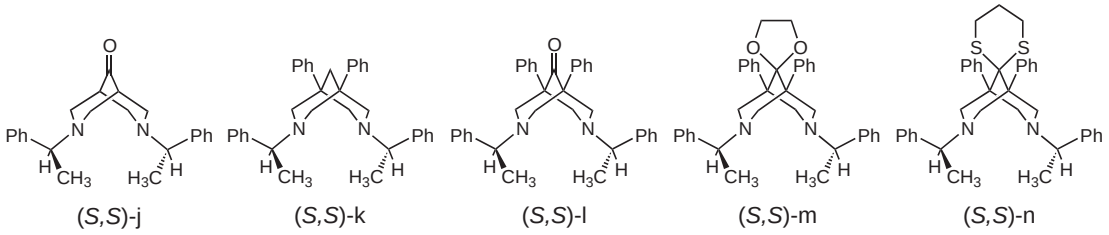

Figure 3.9: Ligands synthesized.

sired L_2PdCl_2 product (Figure 3.11). Unlike the case of (–)-sparteine, the formation of a from ligand o and the $(H_3CCN)_2PdCl_2$ precursor is not exothermic. At the same time, the monodentate complex b is hardly less stable. The lack of multiple fused rings in the proposed ligands also allows the inner piperidine rings to invert and assume the "boat" conformation as in case c. The $Pd(OAc)_2$ complex of o is predicted to be even less stable relative to the acetate complex of (–)-sparteine. Clearly, if bidentate ligands of this type are to be successful a means must be found to improve their stability.

3.4 2nd Generation (–)-Sparteine Mimics

New variations on the bispidine structure were considered in search of ligands which would form robust complexes with palladium while providing reactivity similar to that predicted above. As (–)-sparteine mimics these ligands were intended to remain bidentate throughout a mechanism featuring selectivity-determining β-hydride elimination.

The structure bridging the nitrogen atoms in bispidines was modified with the hypothesis that added flexibility might allow the bound ligand to make stronger bonds to palladium. Unfortunately, the free bispidine framework already orients the nitrogen lone pairs nearly ideally to bind palladium. The flexibility of the ligands in group a of Figure 3.12 instead allows them to relax more (relative to their rigid analogues) when unbound than when coordinated. Hence they are less stable than the bispidines already considered.

Phosphines are known to be oxidized to phosphine oxides in the aerobic conditions employed in these oxidations. Curiously, the chiral phosphine BINAP displayed rates similar to (–)-sparteine, but no selectivity, when screened in Pd-catalyzed kinetic resolutions[31, 32]. It is not known whether BINAP oxidation occurred undetected simultaneously with substrate oxidation, or if the specific

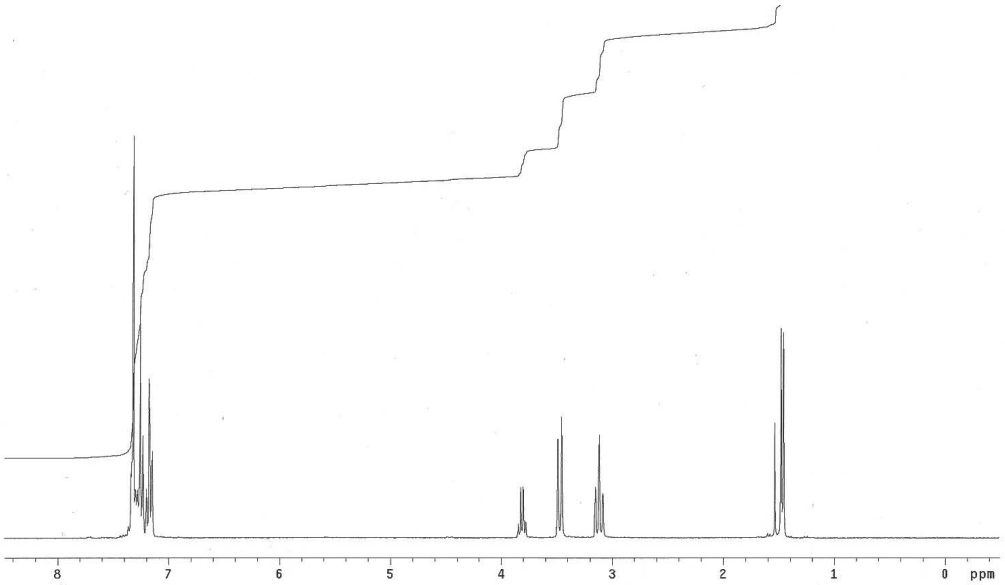

(a)

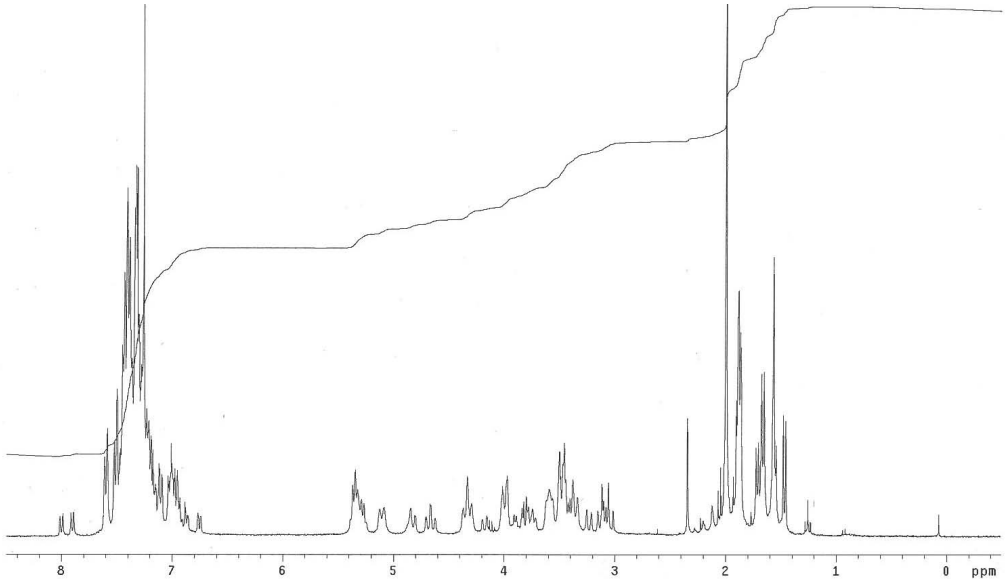

(b)

Figure 3.10: ^{1}H NMR spectra of (a) free ligand k and (b) the reaction products of k and $(H_3CCN)_2PdCl_2$ in $CDCl_3$, courtesy of Jeffrey Bagdanoff.

catalytic mechanism followed by BINAP in this case somehow discourages its oxidation. Our interest in phosphine ligands was therefore tentative, but because of the strength of P-Pd bonds some designs were considered.

Ligands of group b in Figure 3.12 show that replacing the nitrogen atoms of the bispidines with phosphorus indeed yields ligands with superior stability. Unfortunately, the possibility of

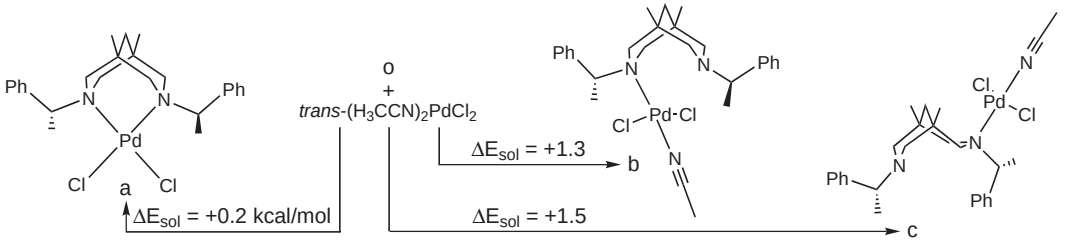

Figure 3.11: Undesirable ligand-metal complexes.

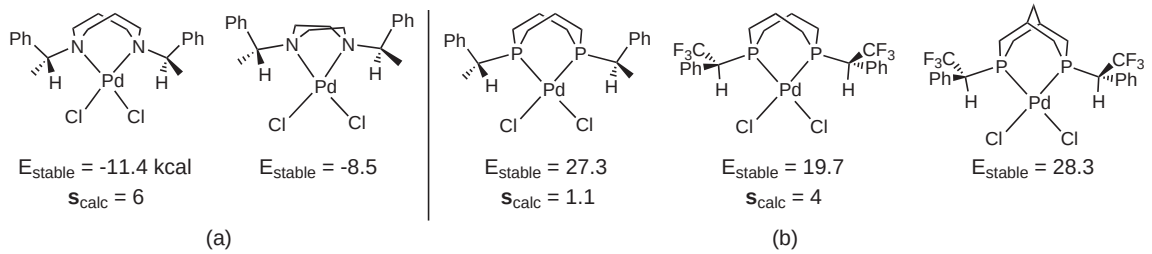

Figure 3.12: Variations on the bispidine framework.

constructing selective ligands by affixing stereogenic carbons to phosphorus is obviated by the nature of phosphorus-carbon bonds. First, C-P-C bond angles (104°–112° in these phosphines) are less than the C-N-C angles in the bispidines (110°–112°), because the greater bond lengths do not require the C-P-C angle to increase as far from 90° to orthogonalize the orbitals on geminal carbons. This means that while the N-C* bonds of the bispidines point the stereocenters somewhat "down" toward palladium (Pd-N-C* angles of 111°), the stereocenters bound to phosphorus are directed farther from the reacting substrate (Pd-P-C* angles of 114°–117°). Second, the greater length of P-C bonds leaves the rotation of the stereocenter unhindered by the ligand backbone. These factors mean that the pocket formed by the phosphine ligands does not firmly impress chirality onto the reaction center, and predicted selectivities are low.

Another approach to improve the stability of the bispidines was to reduce the steric bulk of the pocket where palladium must bind. In ligands p and q (Figure 3.13), one of the stereocenters has been replaced with a methyl group or hydrogen. (p and related C_1-symmetric molecules have been synthesized by Beak, et al.[60]) That the exchange of p and (–)-sparteine on $PdCl_2$ is thermoneutral is in accord with the fact that the two ligands have carbon atoms in the same locations around

the binding pocket. Less hindered q is even more stable. The paring of one stereocenter, however, reduces the predicted selectivity.

Finally, a combination of the stability of phosphines and the potential selectivity of the bispidines was sought. If a synthesis analogous to Beak's in Figure 3.13 is successful beginning with the 4-phosphorinanone r, ligand s would be afforded. This candidate does bind palladium sufficiently as measured by E_{stable}, but the calculated activation energy of the (unselective) monodentate reaction pathway ($E^{\ddagger}_{mono}$ = 12.0 kcal/mol) is less than that for the selective pathway ($E^{\ddagger}_{\beta HE}$ = 18.7 kcal/mol). Evidently strain in the bound ligand is eager to break the Pd-N bond during the reaction. Furthermore, the selectivity through the bidentate path is negligible.

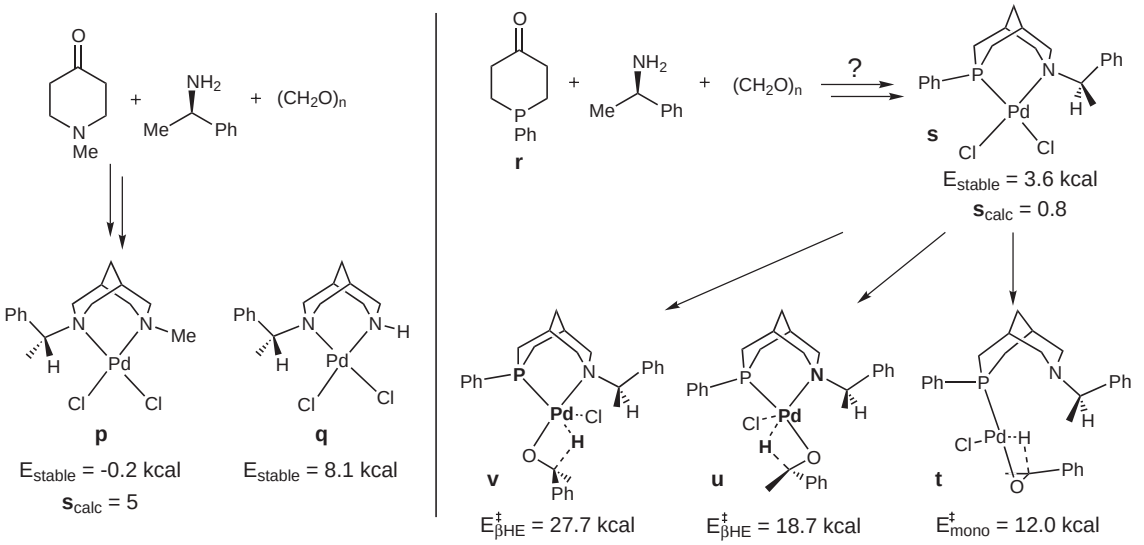

Figure 3.13: C_1-symmetric bispidines and mixed phosphine-amine complexes.

Ligand s illustrates another new concept for using the structure of the ligand to direct the selectivity of a reaction. Section 2.4 explained that in the case of (–)-sparteine the differences among βHE transition state energies (which are the origin of selectivity) are caused by differing interactions between the ligand, anion, and (R) and (S) substrates. Specifically, one face of the ligand is better suited for hosting the anion during βHE, and one site on Pd is favorable for binding the alcohol. The *shape* of the ligand (or ligand-anion combination) is responsible for both these factors. In ligand s, the different *electronic* properties of phosphorus and nitrogen are responsible for strongly

separating the energies of isomeric transtition states. Both hydride and phosphine ligands, unlike amines, display strong *trans* effects. That is, both substituents donate a large amount of charge into the palladium orbital forming the σ-bond, weakening the bond on the opposite side of the metal center to the extent that it shares the same orbital. That the formation of a Pd-hydride *trans* to a phosphine is disfavored because of this phenomenon is evident in the disparate activation energies of isomers u and v in Figure 3.13. The reaction path through v would not be competitive with the path which leaves the hydride *trans* to the amine. This mechanism for splitting the energies of isomeric transition states lies dormant in (–)-sparteine since the two nitrogens are electronically similar. Taking advantage of this degree of freedom might allow us to shift responsibility for destabilizing certain transition states from the *anion* (whose effect is delicately dependent on the solvent) back to the *rigid ligand framework.* The potential of phosphines to be destroyed by oxidation makes them unappealing candidates, but the same effect could be generated by a carbene ligand. N-heterocyclic carbenes have already found utility as stable, electron-rich replacements for phosphines, and have been synthesized in C_1 and C_2 symmetries.

Having broadly surveyed the space of bispidine structures without successfully balancing stability and selectivity, our attention began to turn to a new approach. Many palladium catalysts are known to aerobically oxidize alcohols (primary and saturated substrates as well as benzylic) with no enantioselectivity. Rather than mimicking the catalytic cycle of (–)-sparteine, we consider in the next chapter the possibility of building selectivity into these proven structures.